AEDC-TR-71-172

cy 1

DEVELOPMENT OF CALIBRATION INSTRUMENTATION FOR ABLATION FACILITIES

J. C. Pigott, R. T. Smith, and W. N. MacDermott
ARO, Inc.

September 1971

PROPULSION WIND TUNNEL FACILITY
ARNOLD ENGINEERING DEVELOPMENT CENTER
AIR FORCE SYSTEMS COMMAND
ARNOLD AIR FORCE STATION, TENNESSEE

NOTICES

When U. S. Government drawings specifications, or other data are used for any purpose other than a definitely related Government procurement operation, the Government thereby incurs no responsibility nor any obligation whatsoever, and the fact that the Government may have formulated, furnished, or in any way supplied the said drawings, specifications, or other data, is not to be regarded by implication or otherwise, or in any manner licensing the holder or any other person or corporation, or conveying any rights or permission to manufacture, use, or sell any patented invention that may in any way be related thereto.

Qualified users may obtain copies of this report from the Defense Documentation Center.

References to named commercial products in this report are not to be considered in any sense as an endorsement of the product by the United States Air Force or the Government.

DEVELOPMENT OF CALIBRATION INSTRUMENTATION FOR ABLATION FACILITIES

J. C. Pigott, R. T. Smith, and W. N. MacDermott
ARO, Inc.

FOREWORD

The work presented herein was sponsored by Headquarters, Arnold Engineering Development Center (AEDC), Air Force Systems Command (AFSC), under Program Element 63311F, System 627A.

The results reported herein were obtained by ARO, Inc. (a subsidiary of Sverdrup & Parcel and Associates, Inc.), contract operator of AEDC, AFSC, Arnold Air Force Station, Tennessee, under Contract F40600-72-C-0003. The work was conducted from July 1970 to July 1971 under ARO Project No. PW3107, and the manuscript was presented for publication on June 29, 1971.

This technical report has been reviewed and is approved.

Ules L. Barnwell
Major, USAF
Research and Development Division
Directorate of Technology

Robert O. Dietz
Acting Director
Directorate of Technology

ABSTRACT

Results are presented from a program conducted to develop calibration instrumentation for ablation facilities. The investigation included the development and evaluation of a transient total enthalpy probe, a stagnation point heat-transfer probe, and total pressure probes. A laser shadowgraph was developed for visualization of the flow field. Testing was conducted in the AEDC-PWT Arc Heater Test Unit (5MW). Uncooled probes swept through the flow at high velocity (10 to 40 in./sec) survived the severe heat-transfer conditions and the desired data were obtained. The results of this investigation and a description of the calibration instrumentation are presented.

CONTENTS

APPENDIXES

I. ILLUSTRATIONS

Figure

NOMENCLATURE

C_p	Specific heat
D	Diameter
E	Voltage drop of sample tube
H_o	Total enthalpy
I	Current in sample tube
$\dot{m}$	Sample mass flow rate
p_o	Arc heater chamber pressure
p'_o	Probe stagnation pressure
$\dot{q}_s$	Stagnation point heat-transfer rate
R	Resistance
R_o	Reference resistance (32°F)
T_e	Probe exit gas temperature
T_o	Probe total temperature
T_w	Wall temperature
t	Thickness
V	Volume
x	Distance
αR	Slope of resistivity curve
δ	Boundary-layer thickness
ρ	Density
τ	Time

SECTION I
INTRODUCTION

Recent tests in arc-heated ablation facilities have demonstrated that ablation models often experience ablation rates significantly higher than predicted by Fay and Riddell stagnation point heat-transfer rate theory based on arc heater bulk enthalpy calculated from the arc heater heat balance. In order to make a proper level of prediction, a measurement of local flow conditions including total pressure, total enthalpy, and stagnation point heat-transfer rate must be made. The present methods of using bulk (arc heater heat balance) enthalpy and sonic flow measurements for predicting heating rates are clearly inadequate because of nonuniform enthalpy distributions (Ref. 1).

There have been a number of studies of the problem of direct measurement of local stagnation pressure, heat-transfer rate, and enthalpy in high-shear ablation testing facilities. The high heating rates associated with these facilities destroy most probes in a matter of milliseconds. Since water-cooled steady-state probes have consistently proven inadequate for the flow conditions of interest, other probe concepts were considered. The concept of swept calorimetry using a thin film gage and slug calorimetry to measure heat-transfer rate has been studied experimentally and analytically. The results reported prove the transient characteristics of an ideal null-point calorimeter sufficient to follow a hypothesized heat flux distribution at a sweep speed sufficient to prevent damage to the calorimeter by overheating. The successful use of both swept calorimetry to measure heat-transfer rate and swept large pressure models in the Air Force Flight Dynamics Laboratory (AFFDL) 50-MW Arc Heated Ablation Facility is reported by Aerotherm (Ref. 2).

In high-shear/heat flux facilities, attempts to measure local total enthalpy have been indirect. Most calibrations consist of the measurement of local model stagnation pressure and stagnation heat flux. These, when combined with the proper velocity gradient across the nose of the calorimeter, yield a measure of the stagnation enthalpy. In applying this technique various assumptions must be made which could invalidate the implied enthalpy such as laminar flow, absence of free-stream turbulence, and no arc current flow to the heated, electrically grounded probe surface. Any one or all of these assumptions may be questionable on any particular data run of a facility. At the present time, no method exists for direct measurement of the local stagnation enthalpy in high-shear ablation facilities.

The purpose of the investigation reported herein was to develop instrumentation and data reduction techniques required to calibrate the effluent from arc heaters currently used for ablation testing and for the higher performance ablation facilities under development. The probes developed were a total enthalpy probe, a stagnation point heat-transfer probe, and a boundary-layer stagnation pressure probe. A laser shadowgraph was developed to provide flow visualization. The design, operation, and test results obtained from each of these probes and the laser shadowgraph are presented.

SECTION II
DESCRIPTION OF EQUIPMENT AND INSTRUMENTATION

The primary diagnostic calibration instrumentation developed and used during this study was a total enthalpy probe, a stagnation point heat-transfer probe, total pressure probes, and a laser shadowgraph. The instrumentation was tested in the Propulsion Wind Tunnel (PWT) 5-MW Arc Heater Test Unit (5MW). A description of the calibration instrumentation and the test facility is discussed in this section.

2.1 RESEARCH ARC HEATER FACILITY

The 5-MW research arc heater facility is a continuous flow, high pressure, high enthalpy facility. It contains a gas stabilized Linde N4000 arc heater operating from a d-c power supply, test cell, high-speed model injection system, exhaust duct, and the necessary utilities and instrumentation to operate the facility (see Fig. 1, Appendix I). The Linde arc heater, Fig. 2, consists of two coaxial tubular electrodes separated by an electrically insulated air inlet chamber. Air is injected tangentially into the heater which induces a vortex flow to stabilize the arc and rotate the arc attachment points. The arc-heated airflow is passed through a settling chamber (Fig. 3) and expanded through a M = 2.30 contoured nozzle with a 0.375-in. throat and a 0.619-in. exit diameter. All facility components subjected to critical heating rates are protected by high pressure, high velocity, backside water cooling. The arc-heater power input, mass flow rate, and water coolant losses are monitored so that an energy balance can be made.

The range of the facility flow conditions at the exit of the supersonic nozzle used during the instrumentation development tests was

Total pressure	20 to 60 atm
Model stagnation pressure	10 to 35 atm
Total enthalpy	2000 to 2500 Btu/lb
Mach number	2.30
Velocity	1800 ft/sec (cold flow, no arc) 9000 ft/sec (hot flow)

A high-speed model injection system capable of traversing at controllable speeds up to 80 in./sec was used to sweep the probes through the arc-heated flow.

2.2 TOTAL PRESSURE PROBES

Three total pressure probes were utilized for this study. The first consisted of a commonly used graphite tip probe with a 0.50-in.-diam hemispherical-cylinder-shaped tip. A sketch of this probe is shown in Fig. 4a. The orifice which was located at the probe stagnation point is connected to a strain gage transducer by an 18-in.-long copper tube.

The second probe (designated "boundary-layer probe") had a copper body with a 0.070-in.-diam tip. The tip was small so that local measurements could be made of the flow with a minimum of disturbance. A Kistler Instrument Company Model 603A® crystal gage transducer was selected to be close-coupled to the orifice to obtain adequate responses. A sketch of this probe is shown in Fig. 4b.

A third probe (designated "improved boundary-layer probe") was utilized. This probe, shown in Fig. 4c, was an improved design of the boundary-layer probe previously described. The distance between the probe tip and the pressure transducer was reduced in this probe to a minimum, and the diameter of the inlet passage was held constant from the probe tip to the pressure transducer in order to reduce the volume in front of the pressure transducer. The probe tip was 0.075-in. in diameter, and the probe body was copper.

Obviously, none of these probes could survive steady-state heat flux conditions; therefore, they were swept through the hot jet at high rates of speed. By doing this, profiles of the jet could be obtained in a matter of milliseconds. No visible damage occurred to any of these probes during the survey sweeps of the arc-heated flow.

2.3 ENTHALPY PROBE

The transient enthalpy probe concept, as developed by Cornell Aeronautical Laboratory, Ref. 3, is unique in that it utilizes the transient temperature rise of the gas sampling tube as a measure of sample energy loss. The main components of the instrument are shown in Fig. 5. Basically, the probe consists of an inner sampling tube with an inside diameter D and a wall thickness t. It is protected from extraneous heat loss or gain by means of a thermal-electrical insulating air space which is located between the inner sampling tube and outside shell. This protective shield is an uncooled mass of copper which protects and insulates the sampling tube from the flow stream. A fast-response flow measuring system such as a sonic orifice and a crystal pressure transducer is installed at the exit of the sampling tube. To obtain the enthalpy of a high temperature gas, a sample of the gas is aspirated through the sampling tube for a short time. The sampling tube has a large length-to-diameter ratio and is capable of absorbing most of the heat content of the flow sample. The sampling tube will steadily increase in average temperature. The rate of energy absorption of the tube can thus be inferred from the rate of change of the electrical resistance of the tube.

Ideally, the equation for stagnation enthalpy simplifies to

$$H_o = \frac{(C_p \rho V)_{tube}}{\dot{m}} \frac{1}{\alpha R_o I} \frac{dE}{d\tau} + (C_p T_e)_{gas} \qquad (1)$$

A computer program was written to aid in the design of a reasonable probe configuration. The program was written for fully developed pipe flow in a constant area duct with heat transfer and friction, using the influence coefficients from Shapiro (Ref. 4). Variable air properties were also included. This program provides a conservative design since the heat-transfer rate in the entrance region of the sampling tube is much higher than that predicted by fully developed pipe flow. After considering the nonlinear variation in the temperature-resistivity characteristics of various metals, platinum was chosen as the sampling tube material. The computer analysis pointed out the need for small tubes to reduce response time and a large surface area to remove the heat. Since a single tube did not satisfy these requirements, three tubes in parallel were used. Final design resulted in three tubes, each with a 0.015-in. ID and a 0.005-in.-thick wall. A length of 3 in. was found to be sufficient to remove all of the heat at the design condition: model stagnation pressure of 100 atm and total enthalpy of 4500 Btu/lb. The computed variation of wall temperature down the tube at various times is shown in Fig. 6.

The response of the sampling tube to rapid changes in the inlet flow total pressure and total enthalpy was evaluated using the computer program. An assumed symmetrical profile with a central peak shown in Fig. 7 was entered into the program with the resultant $dE/d\tau$ profile (which is nearly proportional to enthalpy profile) shown in Fig. 8. This profile was obtained by assuming a probe current of 0.50 amp flowing through the tubes. If a larger signal is necessary then much higher currents can be applied through the probe without significant ohmic heating. The characteristic flow time for a slug of gas down the sampling tube varies with inlet flow conditions. At typical ablation facility pressures, the time delay approaches 0.5 msec. The time for the heat from the initial slug of hot gas to transfer radially through the sampling tube was also calculated and is on the order of 0.07 msec. This time is short relative to the time required for a slug of gas to traverse through the sampling tube.

The final design of the transient enthalpy probe is shown in Fig. 9. The major probe components consist of the probe body, an oblate ellipsoid-shaped probe tip, three platinum sampling tubes, a 0.015-in. choked orifice, a piezoelectric pressure transducer, an orifice chamber thermocouple, power and voltage measurement leads, and spacers and insulators. The probe body is a heavy copper structure used both as a thermal protective shield and to protect the probe from the high pressure side loads experienced during probe entry into the flow. An oblate ellipsoid nose tip shape was chosen to reduce the stagnation point heat-transfer rate. It was made separate from the probe body to aid in the probe assembly. The three platinum tubes were spaced in the nose tip to aid in making a 1710°F oven braze joint between the tubes and the nose. Both the temperature and pressure were measured upstream of a choked orifice which was used to measure the probe ingested mass flow rate. A piezoelectric pressure transducer was close-coupled to the orifice to increase its response time. Except for the brazed joint ahead of the resistance-measurement point, the sampling tubes were electrically isolated from the probe body by electrical insulators. The sampling tubes were kept in tension by a compressed spring.

The choked orifice flow measurement system was calibrated using a mass weighing system. The calibration confirmed the calculated flow rate through the choked orifice using a discharge coefficient of 0.82. The sampling tube resistance was measured at various temperatures to confirm the theoretical values for pure, annealed, strain-free platinum as calculated by the Callendar-Van Dusen equation of Ref. 5. A comparison of the AEDC data and data from this reference is presented in Fig. 10. Values for the slope of the AEDC data were used to reduce the probe data to enthalpy.

2.4 STAGNATION POINT HEAT-TRANSFER PROBE

Several techniques are available for measuring local heat flux, but most are limited to heat-transfer rate per unit area less than 1000 Btu/ft^2-sec. The presently accepted standard used to measure high heat-transfer rates is a null-point calorimeter which is swept through the high enthalpy flow at high velocity. This gage is designed using a computer and requires a proprietary technique for manufacture. Its design is based on the premise that there is a unique hole depth for a thermocouple below the heated surface which results in the measured temperature being equal to the undisturbed surface temperature after a small time interval. Knowing the surface temperature as a function of time, the heat flux can be calculated. Another gage which measures surface temperature is a coaxial thermocouple shown in Fig. 11. It consists of concentric Chromel® and constantan rods electrically insulated from each other. The thermocouple junction is made on the exposed surface by mechanical abrasion which smears the thermocouple material across the insulation gap thus creating a thermocouple junction. This type of probe is very inexpensive and was more readily available at AEDC than a null-point calorimeter. For these reasons, this type of gage was evaluated as a possible substitute for the null-point calorimeter gage.

The heat-transfer probe with a coaxial thermocouple installed is shown schematically in Fig. 12a and photographically in Fig. 12b. The probe shape is a 10-deg half-angle cone with a 0.5-in.-diam spherical nose tip. It has an uncooled copper body. The probe was swept through the flow at high speed to obtain local stagnation point heat-transfer rate data. These data can be used to infer enthalpy by using the Fay-Riddell stagnation point heat-transfer equation.

A complicated computer program is necessary to go from the raw data (change in the gage surface temperature with time) to heat-transfer rate when using either a null-point calorimeter or a coaxial thermocouple gage. The program devised by Aerotherm Corporation and named ASTHMA (Ref. 6) is an adequate program for this purpose. The ASTHMA program is a numerical finite difference procedure for solving a one-dimensional heat conduction equation in a solid body given the surface temperature history. By virtue of being a finite difference solution, it lends itself to the incorporation of the variation of properties with temperature of the solid body. From the surface temperature history the heat flux to the body is numerically determined. The major disadvantages of the ASTHMA program are its computational complexity and the fact that it is proprietary.

A program developed for and commonly used in shock tube technology can also be used to calculate heat flux in ablation facilities. This modified shock tube program named AROTHA is a refinement of techniques developed by several investigators. Again the problem is to solve for the heat flux to a semi-infinite body when given the surface temperature as an arbitrary function of time. If the material properties are held constant, an analytical expression for the heat flux can be obtained through considerable manipulation. This expression involves an integral which contains the temperature-time function. Since the data are of arbitrary functional form, and the integral contains a singularity, it can best be evaluated numerically using the method outlined in Ref. 7.

To compare these two programs, raw data taken from the AFFDL 50-MW RENT Facility using a null-point calorimeter were reduced to obtain heat flux using both the ASTHMA and AROTHA programs. The ASTHMA program was run with both constant and variable material properties. These were compared with the constant property AROTHA solution and plotted in Fig. 13. The results compare within 0.5 percent which means that the Aerotherm program, which is both complex and proprietary, is not necessary to reduce this type of data. All of the coaxial thermocouple data were reduced using the AROTHA data reduction program.

2.5 LASER SHADOWGRAPH

Flow visualization in high density arc facilities has for many years been limited to direct luminosity photographs. Conventional shadowgraph and schlieren techniques have not been feasible heretofore because of the intense radiation of light from stagnation regions in the flow. However, the special characteristics of a laser light source provide the possibility of the more conventional techniques because of: (1) narrow band emission which allows selective filtering of the hot gas emission, (2) high intensity to overpower this gas emission, and (3) high brightness (w/cm^2-sr) to allow use of the high power without incurring the image-degrading properties of an extended source.

The operation of any shadowgraph system is based on the small increase with density of the index of refraction of air. Regions of airflow in which there are finite values of second spatial derivative of density ($d^2\rho/ds^2$) will cause differential refractions of light rays, forming bundles of converging or diverging rays. At any image plane, these converging or diverging bundles will create corresponding regions of high intensity and low intensity illumination, i. e., the "shadow" of the

density disturbance. (Regions of constant density gradient, $d\rho/ds$, cause uniform refraction, hence have no effect on light intensity at the image plane.) Since the density profile across a shock wave has symmetrical regions of $\pm d^2\rho/ds^2$, the "shadow" of a shock wave will always consist of closely adjacent dark and light regions at the image plane. Clearly, the intensity of the light and dark regions will vary directly with distance of the image plane from the refracting disturbance, but unfortunately, so will the width of the image. Consequently, in any practical situation, a compromise between image intensity and sharpness must be made, in terms of the image plane distance from the disturbance.

Three laser shadowgraph systems were evaluated, differing mainly in the type of laser used for the light source. The configuration of these three systems is given in Fig. 14. In most conventional shadowgraph systems, the shadow image is recorded by placing a film plate directly at the image plane. In the present case, this was not practical, so a relay lens (L_3) was used to transfer the shadowgraph image from the image plane to the film plane of the camera, which was located outside the test cell.

2.5.1 Lasers

A helium-neon continuous gas laser and a ruby laser operated in both the normal and Q-switched mode were used as light sources. The gas laser was a University Laboratory Model No. 261® which has a continuous 4 mw power output of 6328 Å coherent light. A pinhole spatial filter was used after the gas laser to remove diffraction patterns caused by off-axis modes in the laser. The ruby laser was a standard Korad K-1Q® laser system. The components of this laser system include a Pockels cell Q-switch with a 100-percent reflective mirror, the laser head with a 0.5625- by 4-in. select quality ruby rod, a front reflector, a power supply with electronics, and a water cooler. When the laser was operated in the normal mode, the Pockels cell was not required. By rotating the ruby rod to align its plane of polarization with that of the Pockels cell, the Pockels cell was decoupled from the system. The rated power of the laser system Q-switched is 125 to 150 MW. The pulse duration is from 10 to 12 nsec. In the normal mode the pulse duration is approximately 800 μsec. Operating specifications for the lasers used are presented in Table I, Appendix II.

2.5.2 Telescope

The laser beam was expanded and collimated by the telescope shown in Fig. 14 so that the model and flow field of interest would be illuminated

by a column of parallel light. A diffraction limited negative lens (L_1), antireflection coated for ruby laser light, was used to expand the ruby laser beam. (This lens expanded the beam to a diameter considerably larger than the diameter of the collimating lens. The resultant light loss was unimportant, since ample light was available from the laser.) The beam from the helium-neon laser was expanded by a positive lens of shorter focal length, because of the smaller beam diameter of this laser. This lens was part of the spatial filter. A positive expanding lens could not be used with the ruby laser because the extreme power density at the focus would cause a spark in air. A good quality telescope objective lens (L_2) was used for collimation. A description of these lenses is presented in Table II.

2.5.3 Camera System

A 70-mm camera film magazine was used to hold and advance the film on which the shadowgraph pictures were recorded. The film used with the ruby laser was Afga-Gevaert 10E75® which has very high resolution and is sensitive only to red light. Kodak Tri-X® film was used with the gas laser because the lower power output required a much more sensitive film. Lens L_3, Fig. 14, was the relay lens used to focus the image plane onto the film plane with a magnification of 1.0. The light gathered by the lens was passed through a filter which transmitted the red laser light but blocked the remainder of the visible spectrum. A 2-64 filter was used with the ruby laser and a 2-60 with the gas laser. Neutral density filters (3.0 density) reduced the light intensity from the ruby laser (and from the luminous gas) by a factor of 1000. With the gas laser the light intensity was reduced by a factor of 32 (1.5 density). It was found that an exposure of 10 sec could be used with the ruby laser before the exposure attributable to the gas became objectionable. With the helium-neon laser, some exposure from the gas occurred in spite of the filter because of the lower power and shorter wavelength of this laser.

A shutter with a clear aperture 4.5 in. in diameter was placed immediately in front of the film. When the ruby laser was used, this shutter was operated at its fastest speed, about 0.02 sec, to reduce the exposure to the luminous gas to a minimum. (The length of the exposure to laser light was, of course, controlled by the laser pulse length and not by the shutter.) When the helium-neon laser was used, this shutter served to control the length of the exposure. When the position of the image plane was changed, the film holder, shutter, filters, and lens were moved as a unit so that the image magnification would not be changed.

The probe models were swept through the flow at velocities up to 40 in./sec and the camera shutter and the ruby laser were synchronized to operate when the model was on or near the centerline of the flow. The synchronization was accomplished by means of cam-operated switches. For the shadowgraph pictures using the helium-neon laser, a high-temperature graphite model was injected and stopped on the centerline. This was necessary since the model on a high-speed traverse would have passed completely through the flow during the 0.02-sec shutter opening time.

SECTION III
EXPERIMENTAL RESULTS

The experimental results obtained from the calibration instrumentation probes and the laser shadowgraph previously described are discussed in this section. All probe data presented were collected on an oscillograph or a high-speed digital data system and reduced to engineering units with a computer.

3.1 TOTAL PRESSURE PROBE DATA

The total pressure probes described in Section 2.2 were designed for rapid traverses across arc-heated flows in order that cooling would not be required. At a traverse speed of 30 in./sec, a 0.6-in.-diam jet would be traversed in 20 msec, hence a very short rise time would be required. A 3-msec rise time would result in a loss of about 0.1 in. of the true stagnation pressure profile, and this would seem to form an approximate upper limit to the required rise time.

3.1.1 Graphite-Tipped Probe

The graphite probe, Fig. 4a, was found to have an unacceptably long rise time of 16 msec in a cold flow at 11 atm probe stagnation pressure. (Rise times were measured in cold flows because the boundary layers were thinner than in hot flows, giving a closer approximation to a step-function in pressure.) A 16-msec rise time would result in a loss of nearly 0.5 in. of the 0.6-in.-diam total pressure profile at 30-in./sec injection speed.

To reduce the rise time, the capillary and gage volume were next filled with a low-viscosity oil. The cold flow rise time was reduced to 2.4 msec, within the desired range, but the shape was entirely different

than for the exponentially shaped responses of the air-filled case. The initial rate of rise was appreciably lower than in the air-filled case, suggesting a slow compression of entrained air bubbles in the system by a gradual acceleration of massive slugs of oil. This initial sluggishness was then reversed about midway through pressure responses when a much higher rate of increase began, apparently after compression of all the entrained gas.

The oil-filled probe was then used to measure the total pressure profile for a hot flow at 11-atm probe stagnation pressure and 2250 Btu/lbm stagnation enthalpy. The short rise time observed in cold flow was not obtained in hot flow. In fact, rise times increased to unacceptable levels of 7 to 12 msec. Total pressure profiles measured at 8.23 and 13.42 in./sec are given in Fig. 15a. Clearly, at injection speeds of 30 to 40 in./sec, a large part of the profile would be lost. For comparison with the pressure measurements, a total pressure profile was inferred from boundary-layer calculations. This inferred profile is also given in Fig. 15a. In the hot flow case, the pressure response is also characterized by significant overshooting of the response. The pressure decay as the probe left the jet appeared to begin well ahead of the calculated edge of the boundary layer, a phenomenon which was later explained by the boundary-layer probe. It is not known with certainty why the rise time increased drastically for the hot flow case, but a strong possibility is that of vaporization of oil at the hot end of the capillary. A purely operational problem with the oil-filled probe was frequent spraying of oil out of the probe whenever a region of rapidly decreased pressure was encountered.

3.1.2 Boundary-Layer Probe

This probe, Fig. 4b, represents an attempt to obtain the necessary short rise times by use of a piezoelectric transducer mounted within the probe itself and without resort to oil in the cavity. In the cold flow at 11-atm probe stagnation pressure, this probe was found to have a rise time of 3 msec — at the upper limit of the acceptable range. Furthermore, this favorable rise time appeared to be maintained in hot flow at 22-atm probe stagnation pressure and 1960-Btu/lbm stagnation enthalpy, Fig. 15b. There are only minor differences in the profiles obtained in two different directions, which indicates adequate response. The profile displays a boundary layer approximately 0.070 in. thick and a reasonably uniform core flow. High-frequency oscillations are also apparent in the core. Since the probe traverse was made 0.1 in. downstream of the end of the nozzle, there is also an intervening transition region between the edge of the test rhombus and the edge of the boundary layer, which is the expansion zone required to

match the jet pressure to the ambient pressure outside the nozzle. This zone is obviously the explanation for the "premature" pressure decay observed with the graphite probe. The boundary-layer thickness was verified by the laser shadowgraph.

3.1.3 Improved Boundary-Layer Probe

By a further reduction in volume between the probe orifice and the pressure transducer, Fig. 4c, an even shorter rise time was obtained. In the standard 11-atm cold flow test, the improved boundary-layer probe displayed a rise time of only 0.4 msec, which is approaching the limits of the system electronics and readout instrumentation. There is some evidence, however, that this rise time may be too short, since the system is observed to "ring" when exposed to the sharpest pressure pulses at maximum injection speeds. The "ringing" corresponds closely to the natural pneumatic frequency of the cavity and could presumably be eliminated by design of a zig-zag capillary. A series of total pressure profiles obtained with this probe in a cold coaxial nozzle flow at injection speeds of 2.3 to 36.5 in./sec is given in Fig. 15c. This flow is the result of a coaxial expansion of two separate supersonic streams, and the mixing region between them is clearly defined and faithfully reproduced over this range of injection speeds. This probe was subsequently used with an arc-heated inner core flow in the coaxial nozzle, and the results were entirely satisfactory.

3.2 ENTHALPY PROBE DATA

The transient enthalpy probe was subjected to the arc-heater flows at p_o' = 10 to 30 atm, heat balance enthalpy of 2070 to 2160 Btu/lbm at sweep rates of 25 to 33 in./sec. The voltage drop of the tube was recorded as a function of time in analog form on an oscillograph recorder and in digital form on magnetic tape. Both sources of data were used in evaluating the probe.

Aside from a quantitative comparison with other enthalpy measurements, the probe design was found to be quite satisfactory from a functional standpoint. Its physical ruggedness was adequate to withstand the large side loads imposed during injection into the high pressure jet, and the nose tip was sufficiently blunt that absolutely no erosion or ablation was experienced. A considerable advantage in simplicity was represented by the absence of any cooling water requirements. Not only was there no need for an extensive cooling water supply system, but there was also no need for concern over possible water leaks.

The quantitative output of the probe ($dE/d\tau$), although clearly related in some way to the stagnation enthalpy of the gas, was not entirely satisfactory and did not follow the simple response theory of Eq. (1) in Section 2.3. The uncorrected enthalpy profile, Fig. 16, was only approximately in the expected range and displayed rather drastic differences from the expected shape. Since a stilling chamber upstream of the nozzle was in use, a reasonably uniform total enthalpy profile was anticipated. Instead, the profile was highly asymmetrical. Values as high as 5000 Btu/lbm on the initial part of the profile and as low as 500 Btu/lbm on the terminal part of the profile were found. It was encouraging, however, that there appeared to be a partial levelling out of the profile in the vicinity of the expected value of 2000 Btu/lbm.

An analysis was made of the possible corrections to the simple output equations. Three corrections were found which were of appreciable magnitude:

1. Pneumatic Lag

   By inspection of individual output parameters recorded for the probe, it was determined that the initial overshoot of enthalpy was associated with a lag in the indicated sample mass flow rate ($\dot{m}$) during the period the probe was entering the jet flow. This was a pneumatic lag in the capillary connecting the metering orifice chamber with the pressure transducer and was much less noticeable on the departure of the probe from the jet because the capillary and probe volume were already up to pressure at this point. By assuming that the sample mass flow was directly proportional to the pitot pressure, a correction for the pneumatic lag was made for that part of the profile for which pitot pressure was known with reasonable accuracy. This mass flow correction is indicated on Fig. 16.

2. Nonlinear Resistivity

   Further inspection of the individual output parameters of the probe showed that the average sample tube temperature was rising to values at which the tube resistance should be considered a nonlinear function of temperature. In this range the measured sample tube resistance was no longer uniquely related to the average tube temperature, but depended upon the temperature distribution as well. It was assumed that the nonlinear character was represented by

$$R = R_0 (1 + \alpha T + \beta T^2)$$

where α = 0.00392/°C and β = -5.88 x 10^{-7}/(°C)^2. It was found that the temperature distribution given by the theoretical calculations of tube response, Fig. 6, displayed a self-similarity in time. Using these profiles, a nonlinearity correction to the enthalpy probe output was obtained which amounted to a 30-percent correction at an average tube temperature of 600°F. Since the average temperature increased during the traverse of the probe through the jet, this correction also increased in magnitude during the traverse, which was in the direction of a more uniform enthalpy profile. The correction is indicated in Fig. 16.

3. Heat Losses

It was apparent that there were several possible types of heat loss from the sampling tube: conduction at the tube supports, conduction along signal and power leads, and radiation to the main body of the probe. Further study suggested a very simple procedure by which most of these losses could be evaluated. At the instant that the probe passed out of the jet the shape of the tube voltage versus time curve on the oscillograph record was found to change suddenly from a very high rate of increase attributable to sampling of hot gas to a relatively small rate of decrease which obviously represented the residual heat loss from the tube with $\dot{m}$ = 0. The ratio of the $dE/d\tau$ immediately before and after this point then provided a direct indication of the ratio of heat losses to the heat transferred to the probe from the gas sample. This loss was also assumed to be proportional to the average tube temperature, giving another correction which grew in magnitude during the traverse through the jet, as shown in Fig. 16. There was one source of heat loss which was not accounted for by this procedure: namely, the radial conduction into the probe support structure at all points ahead of the metered section of the probe.

The resulting total enthalpy profile, after performing the three corrections, Fig. 16, was found to be much closer to the expected profile than was the uncorrected profile. It can be seen that a reasonable degree of flatness was obtained, and that on the side of the profile where the probe emerges, and where there is little or no lag in $\dot{m}$, a reasonable

boundary-layer profile resulted. However, the mean level of the profile is 1748 Btu/lbm, 15 percent lower than the heat balance enthalpy. It is anticipated that a further analytical correction will be made to allow for the remaining heat loss ahead of the metered section of the probe; this should reduce this discrepancy between the probe and the heat balance enthalpy.

3.3 STAGNATION POINT HEAT-TRANSFER PROBE DATA

Typical heat flux data obtained with the coaxial thermocouple stagnation point heat-transfer probe are shown in Fig. 17. The flow conditions for the data presented were a total pressure of 21.8 atm and a total bulk enthalpy of 2070 Btu/lbm, which were obtained from a heat balance on the arc heater. The probe sweep rate was 37.5 in./sec. The thermocouple temperature as a function of the probe position in the flow is shown in Fig. 17a. The corresponding heat-transfer rate to a cold (70°F) constant temperature surface was calculated using the AROTHA data reduction program. The flat heat-transfer profile shown in Fig. 17b is typical of profiles obtained from this arc heater when using a stilling chamber. The total enthalpy of the arc-heated flow corresponding to the heat-transfer rate shown is also presented. The enthalpy was calculated using the Fay and Riddell heat-transfer theory. The centerline heat-transfer rate corresponds to an enthalpy of 3300 Btu/lbm. This is 60 percent higher than the 2070 Btu/lbm bulk enthalpy calculated from the heat balance on the arc heater with stilling chamber. Many more profiles were obtained and were observed to be typically flat as shown in Fig. 17b.

3.4 LASER SHADOWGRAPH DATA

A series of shadowgraphs taken of the flow field around the diagnostic calibration instrumentation probes is shown in Figs. 18 through 21. Shadowgraphs taken of the flow field about the graphite tip total pressure probe are shown in Fig. 18. The purpose of this series of shadowgraphs was to determine the effect of image plane location on sensitivity and resolution. These shadowgraphs were taken in cold flow at 11-atm probe stagnation pressure.

It can be noted from the shadowgraphs that the short pulse width of the ruby laser (10 to 12 nsec) stopped the motion of both the model and the flow. The sensitivity of the shadowgraph is observed to increase as the image plane is moved away from the model. However, increased sensitivity occurred at the expense of model and shock wave definition.

Since a relay lens was used, it was possible to move the image plane past the flow centerline in the light source side of the flow. As the image plane was moved from one side of the model to the other, the light and dark areas of the visible shock waves were reversed.

Figure 19 is a series of pictures taken of the same model again in the Q-switched mode, but in arc-heated flow at 11-atm probe stagnation pressure. It can be observed that because of the lower density of the arc-heated flow, the bow shock is not as pronounced as for the corresponding cold flow case.

If one compares hot flow and cold flow pictures taken at the same image plane location, it appears that in the hot flow pictures, the turbulence is somewhat less distinct, but the shock waves are much less distinct. It seems possible that most of the turbulence originates in the boundary layer between the hot and cold gas where the density is relatively high, whereas the shock waves originate, of course, within the hot gas where the density is low. This would explain the reduced visibility of the shock waves against the turbulent background in the hot flow pictures.

Figures 18c, 20a, and 20b show the effect of the different light sources under cold flow conditions. All were taken with the image plane 2.0 in. from centerline. The principal effect of increasing exposure length is to "time average" the picture. This causes moving features such as turbulent eddies to become less distinct as exposure length increases, but stationary features such as shock waves remain at about the same contrast.

The turbulence recorded in Fig. 18c (Q-switched mode) obscures most of the details of the shock wave pattern. In Fig. 20a (normal mode) most of the turbulence has been averaged out, and a much more detailed picture of the flow can be seen. However, at this exposure time (about 800 μsec) motion blurring of the model begins to be troublesome. In Fig. 20b (gas laser) no trace of turbulence can be seen, and very fine structure is visible in the shock pattern close to the model.

On the other hand, the boundary between the flowing and stationary gas seems to be visible mainly because of the difference in turbulence level. The boundary of the flow is clearly visible in Fig. 18c, but has entirely vanished in Fig. 20b. The exact boundary of the flow is uncertain in Fig. 20a.

It is somewhat surprising that any turbulence at all is visible in Fig. 20a considering the length of the exposure. The structure which can be seen must be moving with a velocity of 10 ft/sec or less.

This may lend some support to the idea that much of the turbulence is associated with the boundary layer and not with the bulk of the flowing gas.

Figures 21a, b, and c compare Q-switched, normal mode and CW light sources for the hot flow case (p_o' = 11 atm). The image plane is again 2.0 in. from centerline. The observations which were made in connection with the cold flow pictures again apply. The principal difference between the cold and hot flow pictures is that less detail is visible in the shock pattern in the hot flow case. It appears that it might be advantageous to increase the sensitivity of the shadowgraph system for the conditions of Fig. 21c since the turbulence has been eliminated.

Figures 21c and d show what can be accomplished by filtering. Figure 21c was taken with a filter which was cut off quite sharply at a wavelength slightly shorter than the laser wavelength. Since most of the radiation from the model is at shorter wavelengths, most of this radiation was eliminated. Figure 21d was taken with a filter which cut off much more gradually. Radiation from the model obscures much of the flow. At higher stagnation pressures, even more detail was lost.

In this case, the results obtained with the sharp cut-off filter are probably satisfactory, even though the radiating model produced some exposure. Had the sharp cut-off filter been inadequate, an interference filter could have been used. This is a very narrow bandpass filter which would eliminate light at both longer and shorter wavelengths and would probably cut the light from the model by at least an additional order of magnitude. Unfortunately, interference filters are expensive and difficult to use.

SECTION IV
DISCUSSION

The major interest in probe development centered around the transient enthalpy probe because of the general lack of instrumentation capable of measuring this parameter in high-performance arc heaters used for ablation testing. Such facilities typically have jet diameters of less than 1 in. and are operated without stilling chambers to maximize the enthalpy level. Without the stilling chamber, the enthalpy profile is frequently quite nonuniform and the bulk enthalpy given by heat balance is of little value in analyzing model heat transfer or ablation data. Lack of a local measurement of stagnation enthalpy is one

reason why standard ablation models are frequently run for comparison purposes in ablation facilities.

Enthalpy measured by the stagnation point heat-transfer probe, the transient enthalpy probe, and the sonic flow equation is compared with enthalpy measured from the arc-heater heat balance in Fig. 22. It can be noted from this figure that enthalpy calculated from the sonic flow equation is in close agreement with the arc heater heat balance which is typical when a stilling chamber is used. The transient enthalpy probe data indicate a lower enthalpy than the arc-heater heat balance. As noted in Section 3.2 previously, some of this discrepancy can be resolved by accounting for the heat loss ahead of the metered section of the sample tube. The enthalpy probe values in Fig. 22 have already been corrected for pneumatic lag, nonlinear resistivity, and heat losses downstream of the metered section. The stagnation point heat-transfer probe indicates an enthalpy much higher than the energy balance. The enthalpy was calculated using the Fay and Riddell stagnation point heat-transfer equations for enthalpy. The high indicated enthalpy obtained by this method may be attributable to flow conditions (for example, turbulent flow) for which the Fay and Riddell equation does not apply.

SECTION V
CONCLUDING REMARKS

The major problem in calibrating ablation facilities is the design and fabrication of small probes which can survive the hostile environment. A method of circumventing the heat-transfer and cooling problem of small steady-state probes is to traverse the probes through the flow at speeds sufficient to prevent probe destruction. This method was demonstrated with uncooled total pressure probes, an enthalpy probe, and a stagnation point heat-transfer probe.

Several total pressure probes were evaluated. A specially designed boundary-layer probe with an onboard piezoelectric pressure transducer, short-coupled to a small diameter (0.075-in.-OD) probe tip, displayed a rise time of 0.4 msec at 11 atm probe stagnation pressure. The probe size and response time were adequate to measure small area total pressure disturbances at sweep rates which prevent probe destruction in high pressure-enthalpy ablation facilities.

A transient enthalpy probe was designed and tested. The uncooled calorimetric probe was traversed through the flow in less than destruction time. The probe demonstrated a good enthalpy response by following

the flow profiles obtained by the pressure and heat-transfer probes and by its response to arc-heater fluctuations. After applying corrections for pneumatic lag, nonlinear resistivity, and heat loss, the enthalpy level measured with the probe was 15 percent less than that obtained from the arc-heater heat balance or the sonic flow equation. Much of this remaining discrepancy can be resolved by applying a final correction to account for heat loss at the tip of the probe, ahead of the instrumented section of the sampling tubes.

Stagnation point heat-transfer rates, calculated by computer from the coaxial thermocouple probe data, show that this type of probe has a very fast response time, and the heat-transfer rates follow the arc-heater fluctuations. The enthalpy inferred from the data through Fay and Riddell equations is considerably greater than measured by the enthalpy probe or calculated by the sonic flow equation and the arc-heater heat balance. This difference can be attributable to several factors not accounted for when using the Fay and Riddell equation.

It was shown that shadowgraph pictures may be obtained in an arc-heated facility, in spite of the intense light radiated by a probe or model in the flow, if a laser is used as the light source. It was found that using a ruby laser in the Q-switched mode (10-nsec pulse width), the laser "froze" all of the details of the flow at 9000 ft/sec, including both the shock pattern and the turbulence. The longer exposures obtained with the ruby laser in the normal mode and with a continuous gas laser produced time-averaged pictures in which moving features of the flow such as turbulence are averaged out while stationary features such as shock waves are not.

Excellent pictures of the flow were obtained under cold flow conditions. Under hot flow conditions, turbulence tended to obscure shock patterns. The best pictures of shock patterns in the hot flow were obtained with the continuous laser source, but in most cases, the boundary between the flowing and the stationary gas could not be seen. The boundary was clearly visible in pictures taken with the Q-switched laser because of the higher turbulence of the flowing gas.

REFERENCES

1. Folck, J. L. and Smith, R. T. "Calibration of the AFFDL 50 Megawatt Arc Heated Hypersonic Wind Tunnel with a Two-Foot Nozzle." AFFDL-TR-69-36, August 1969.

2. Rindal, R. A., Kennedy, W. S., and Powers, C. A. "A Recommended Calibration Program for the AFFDL 50MW RENT Facility." Aerotherm Report 69-55, August 1969.

3. Vassallo, F. A. "Miniature Enthalpy Probes for High Temperature Gas Streams." ARL-66-0115, June 1966.

4. Shapiro, A. H. The Dynamics and Thermodynamics of Compressible Fluid Flow. The Ronald Press Company, New York, 1954.

5. Rosemount Engineering Company. "A General Technical Bulletin on Platinum Resistance Temperature Sensors." Bulletin 9612, 1962.

6. Moyer, C. B. "Axi-Symmetric Transient Heating and Material Ablation Program (ASTHMA) Description and User's Manual." Aerotherm Report No. 68-67, January 1968.

7. Felderman, E. J. and Cook, W. J. "Reduction of Data from Thin Film Heat Transfer Gages: A Concise Numerical Technique." AIAA Journal, Vol. 4, No. 3, March 1966, p. 561-562.

APPENDIXES

I. ILLUSTRATIONS
II. TABLES

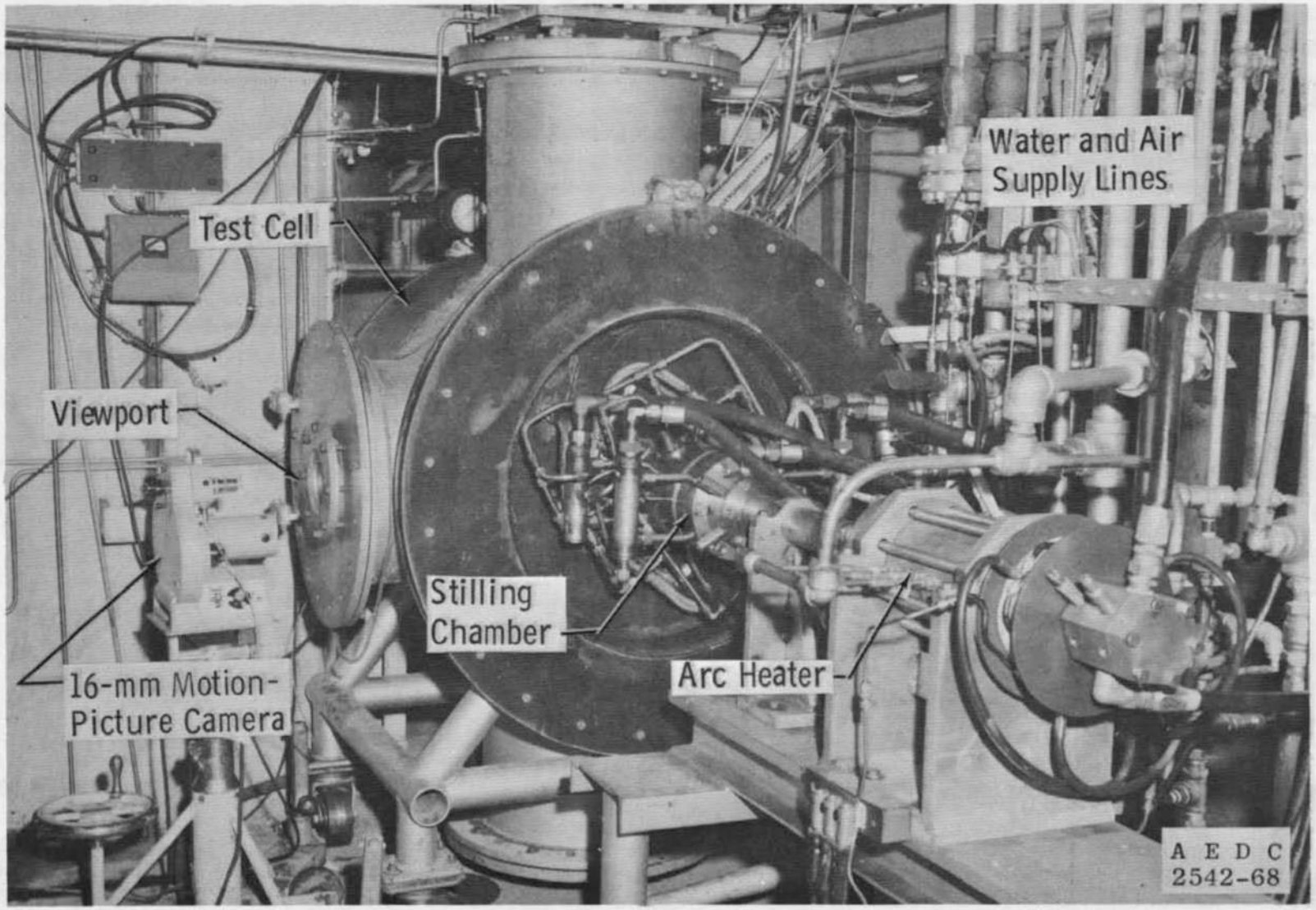

Fig. 1 Research Arc Heater Facility

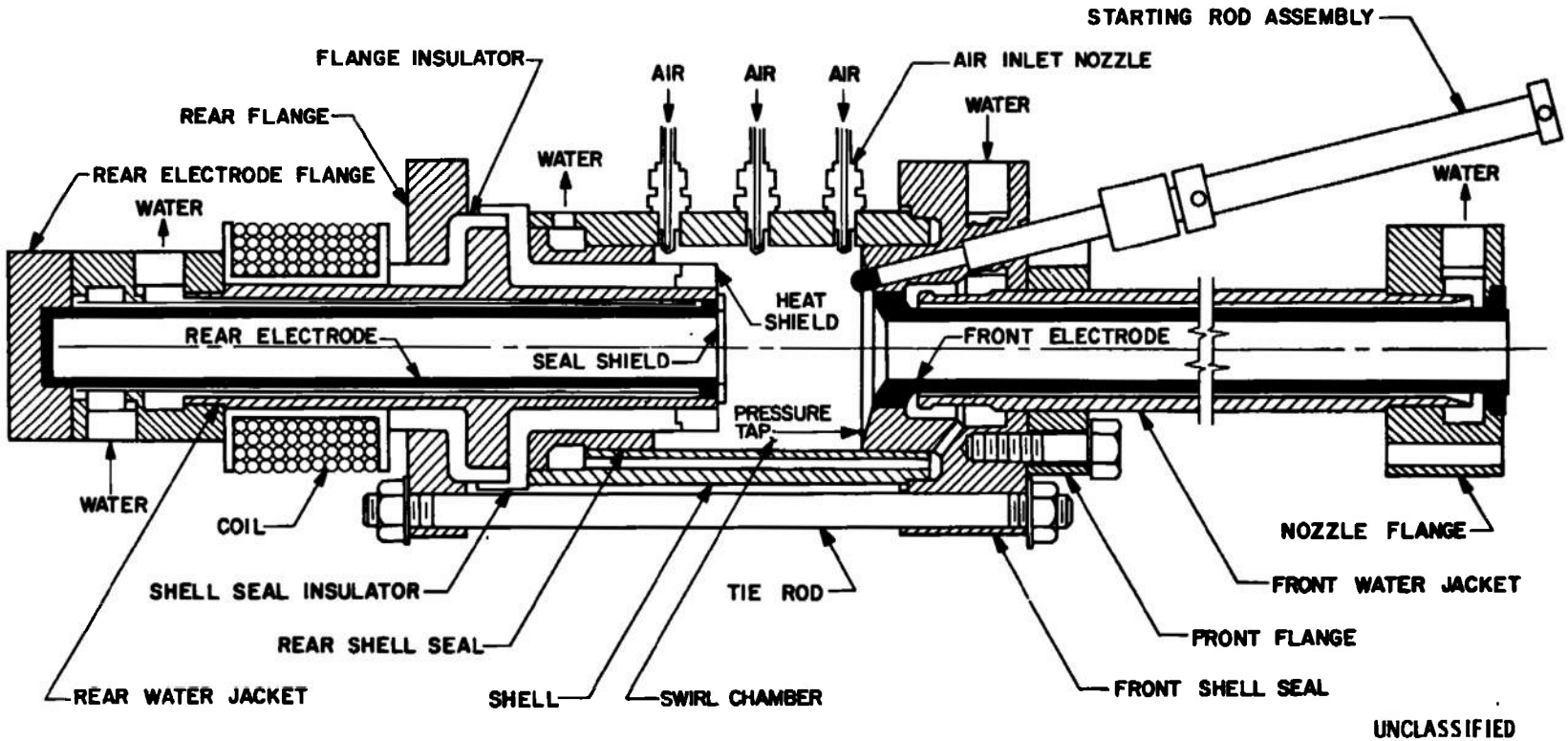

Fig. 2 Arc Heater Schematic

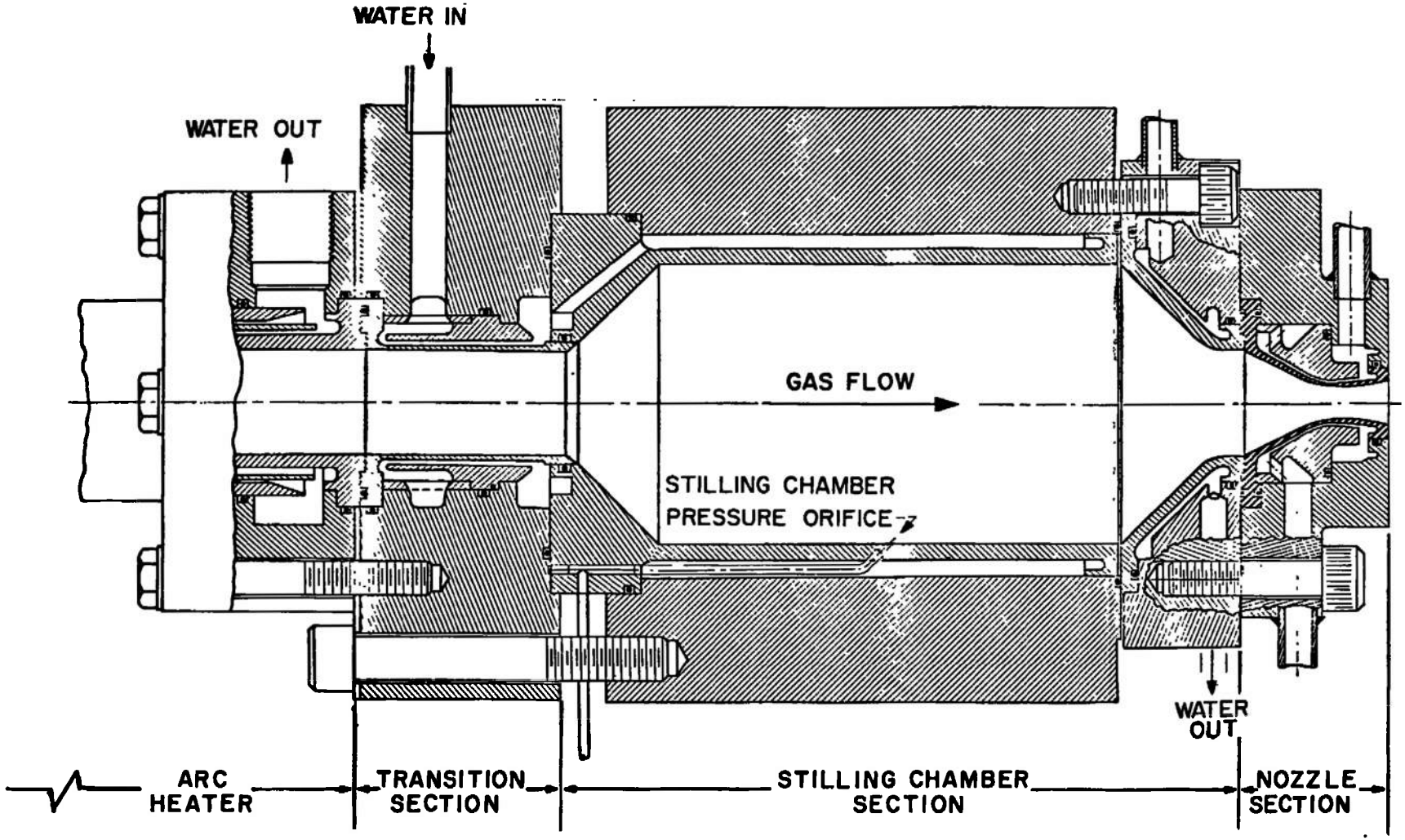

Fig. 3 Arc Heater Stilling Chamber and Nozzle

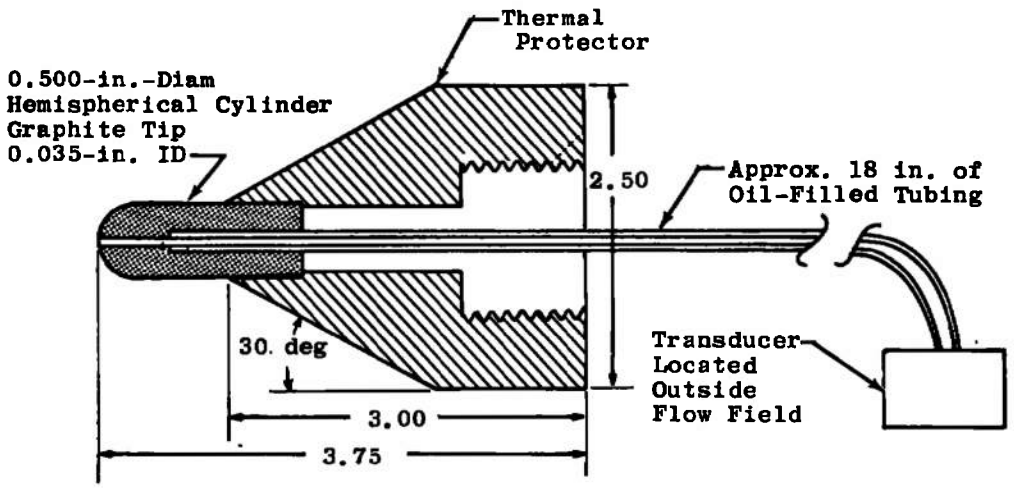

a. Graphite Probe

Note: All Dimensions in Inches

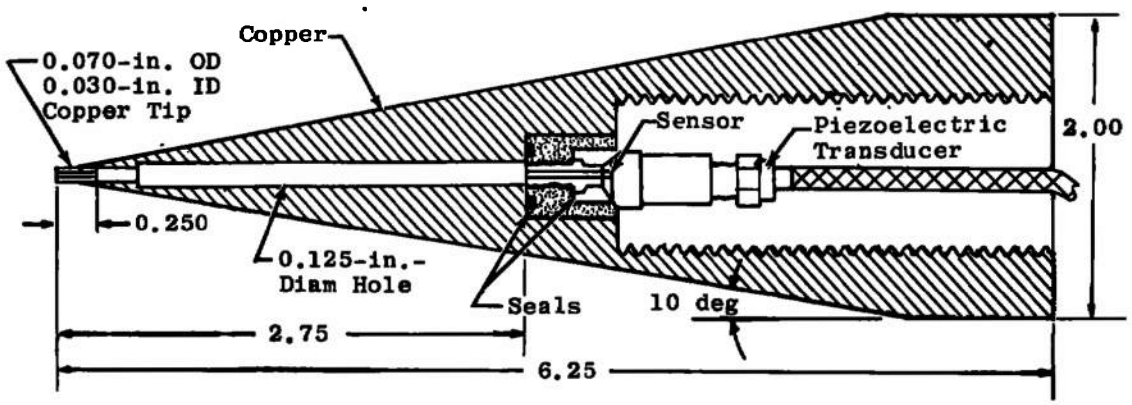

NOTE: All dimensions
in inches.

b. Boundary-Layer Probe

Fig. 4 Total Pressure Probes

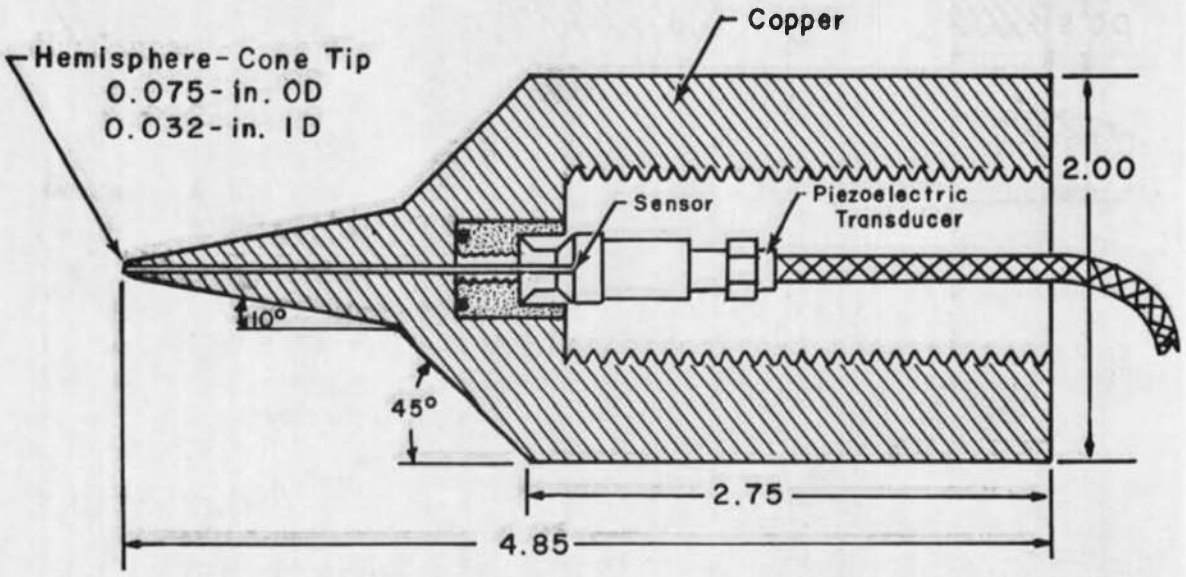

NOTE — ALL DIMENSIONS IN INCHES

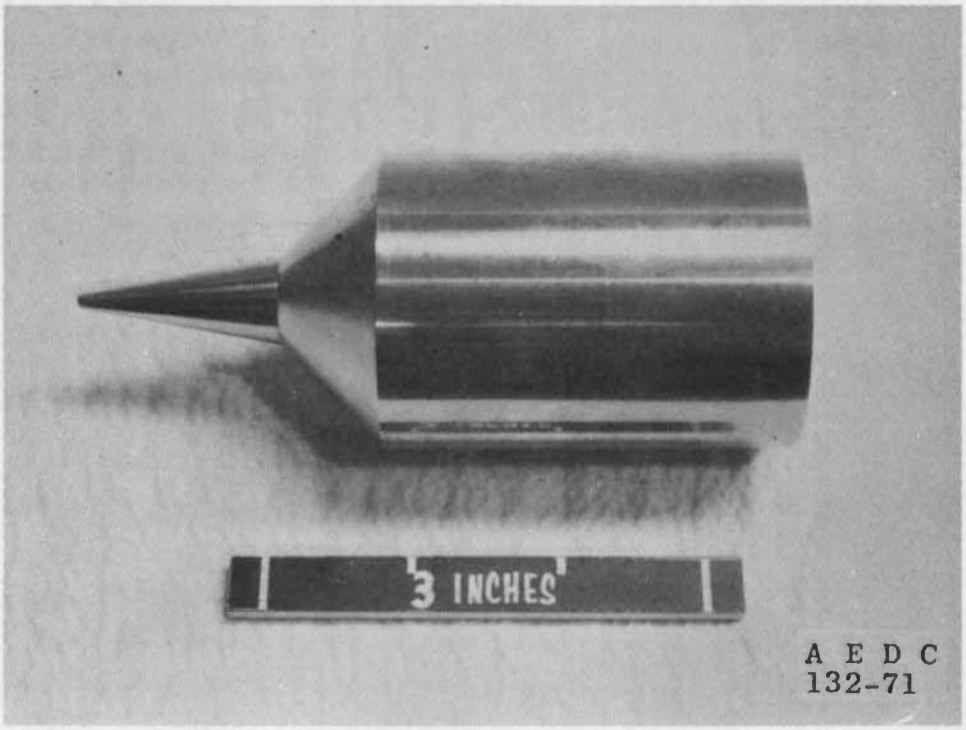

c. Improved Boundary-Layer Probe
Fig. 4 Concluded

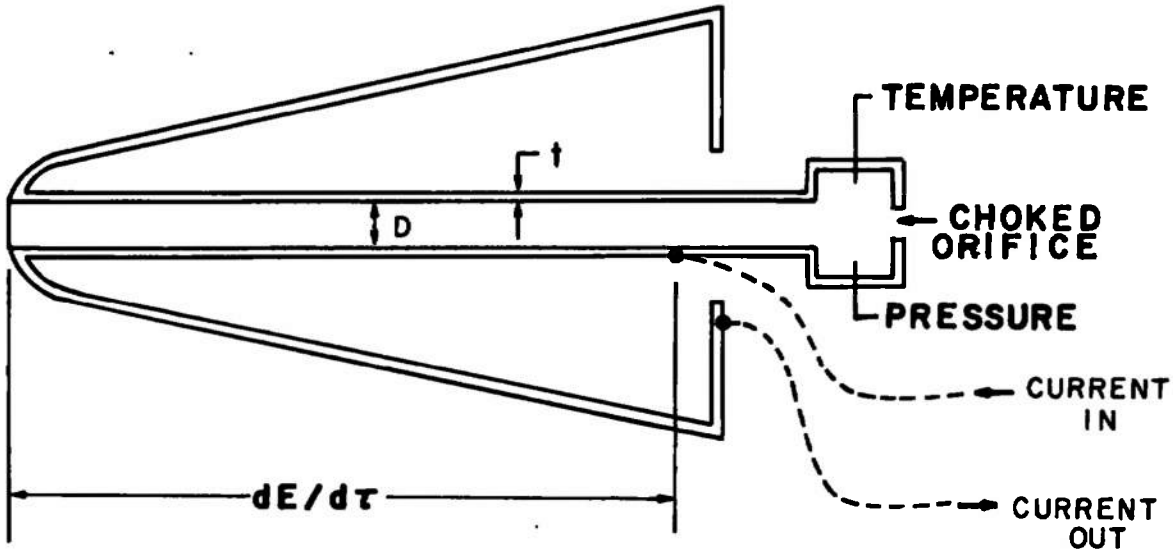

Fig. 5 Transient Enthalpy Probe Concept

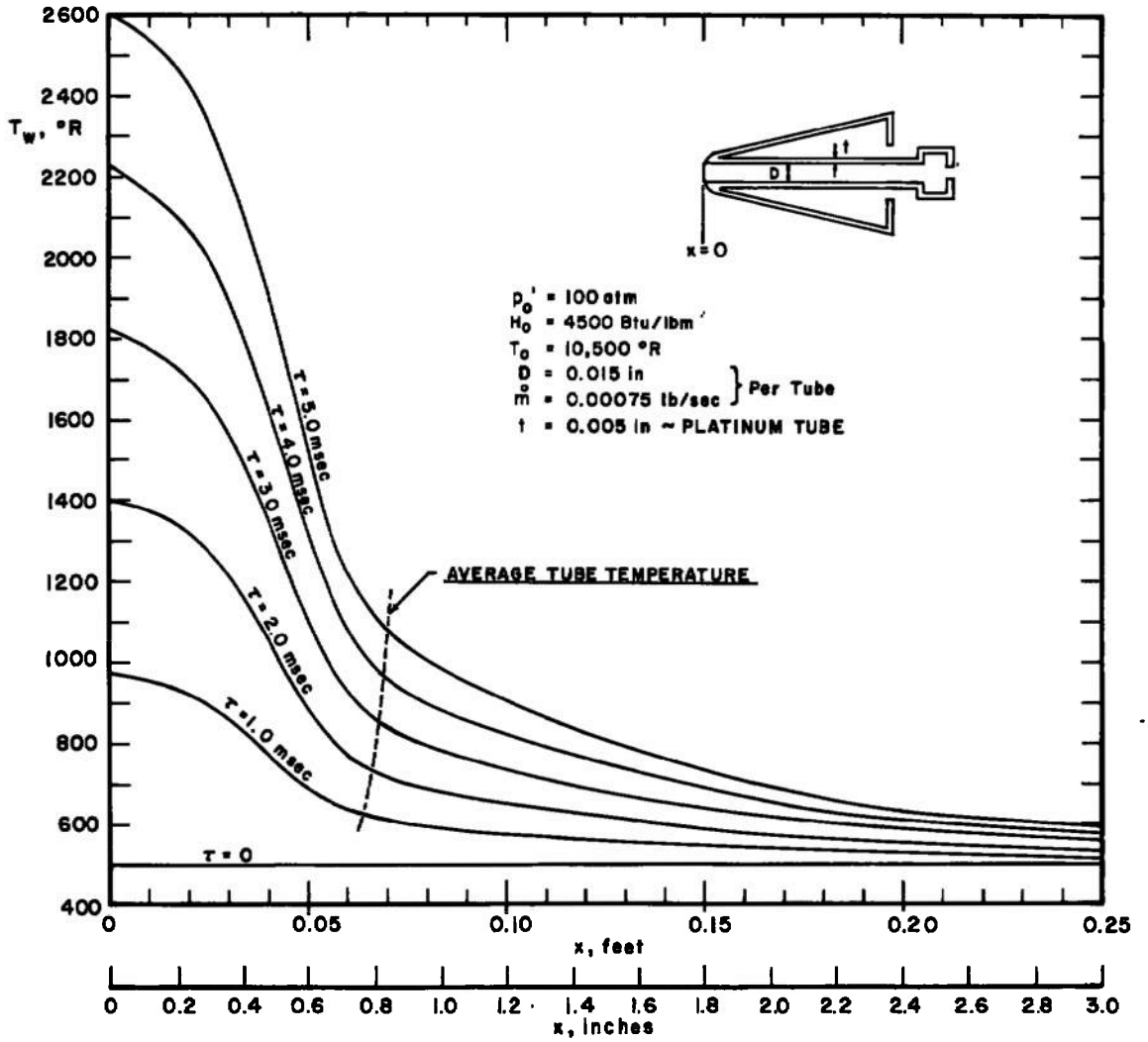

Fig. 6 Computed Variation of Transient Enthalpy Probe Sampling Tube Temperature with Time

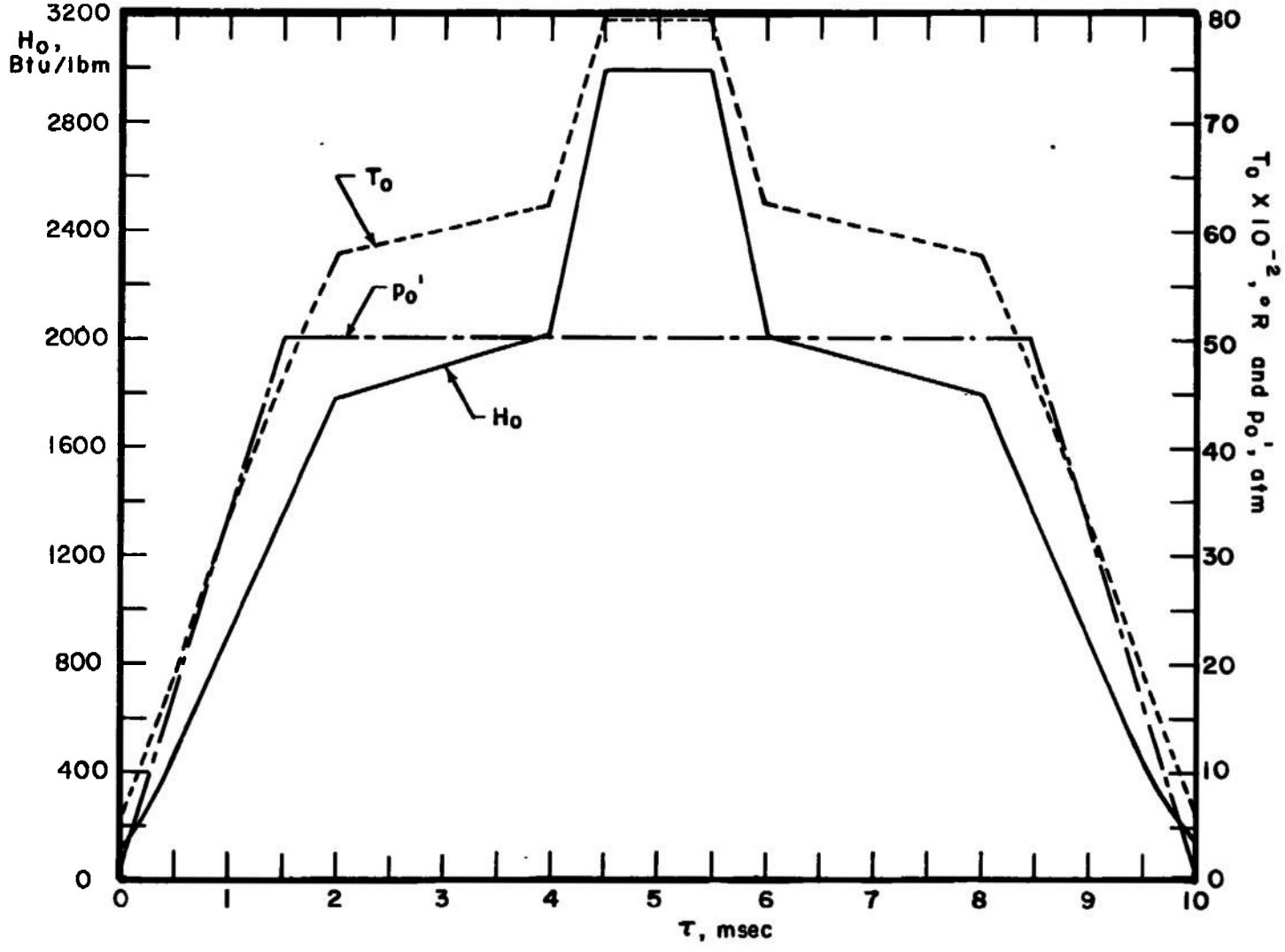

Fig. 7 Computer Input Data for Calculating the Response of the Transient Enthalpy Probe Sampling Tube

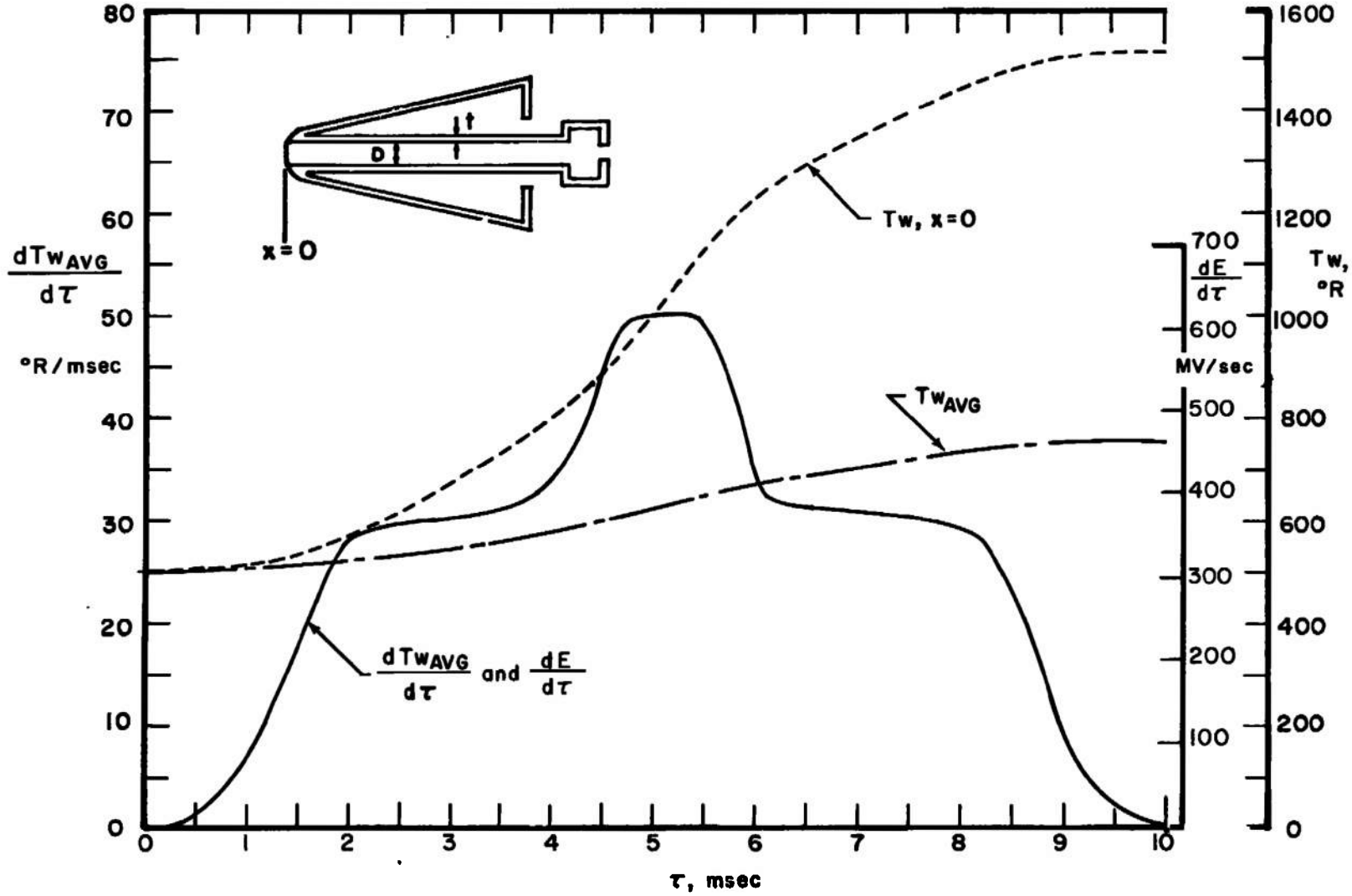

Fig. 8 Transient Enthalpy Probe Sampling Tube Response Calculated from the Computer Input Data of Fig. 7

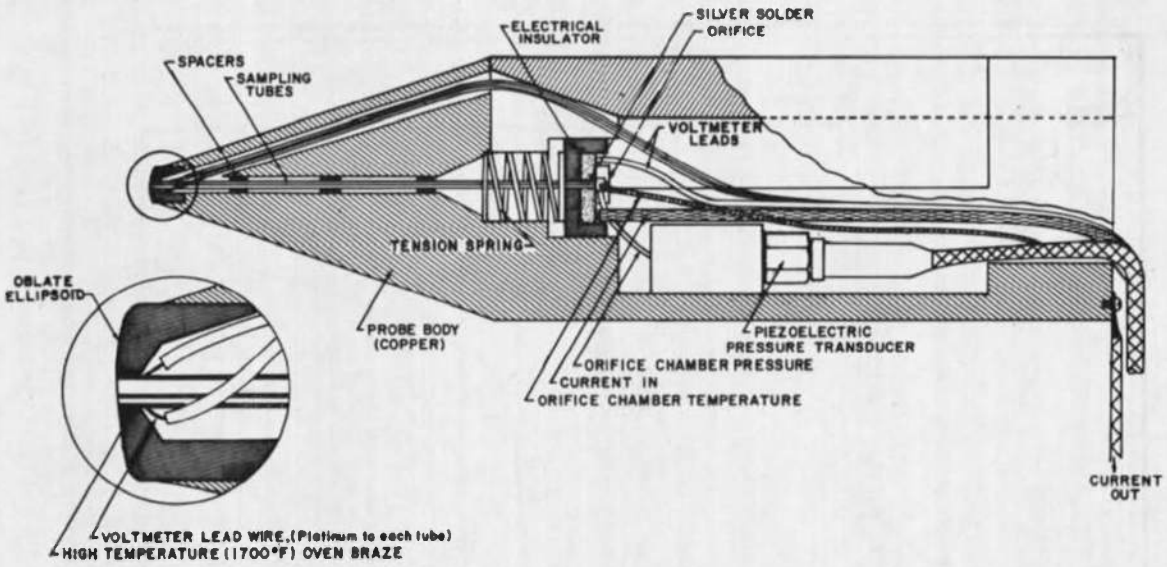

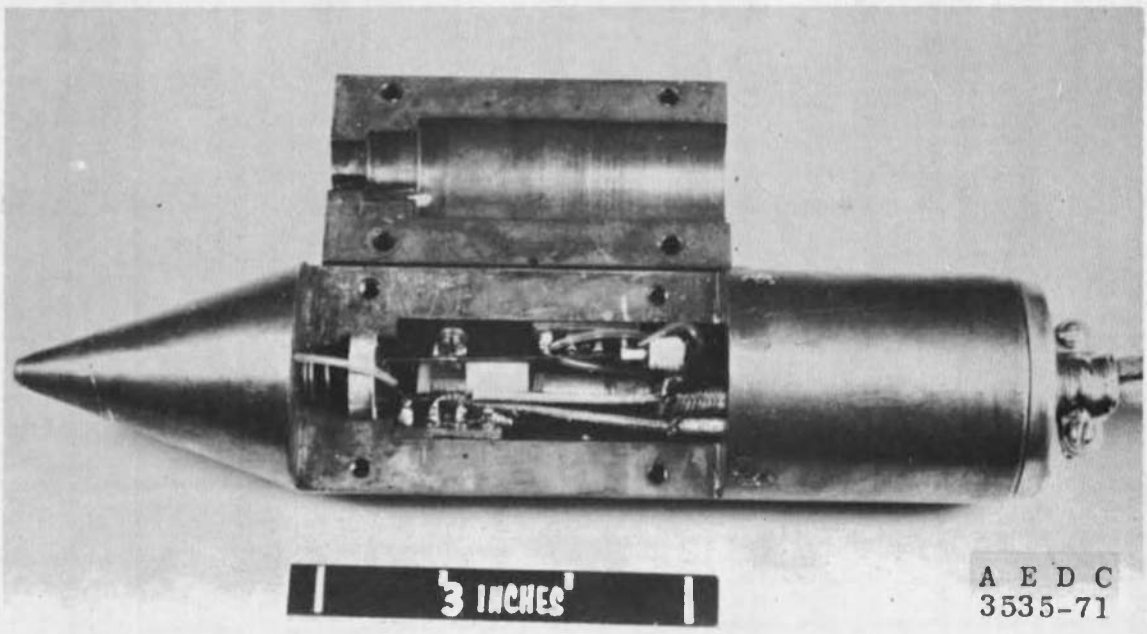

Fig. 9 Transient Enthalpy Probe

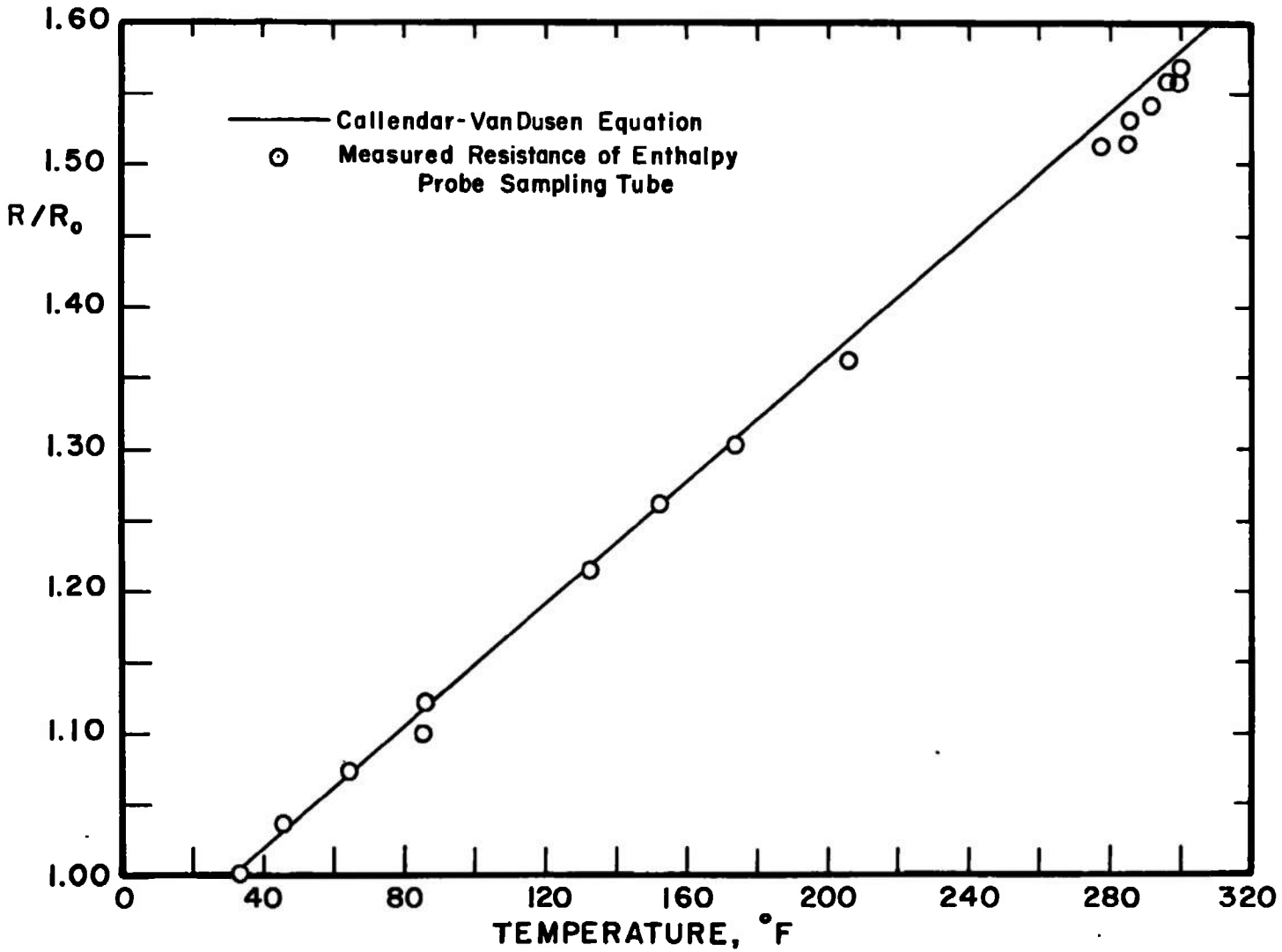

Fig. 10 Comparison of the Transient Enthalpy Probe Sampling Tube Measured Resistance and the Callendar-Van Dusen Equation

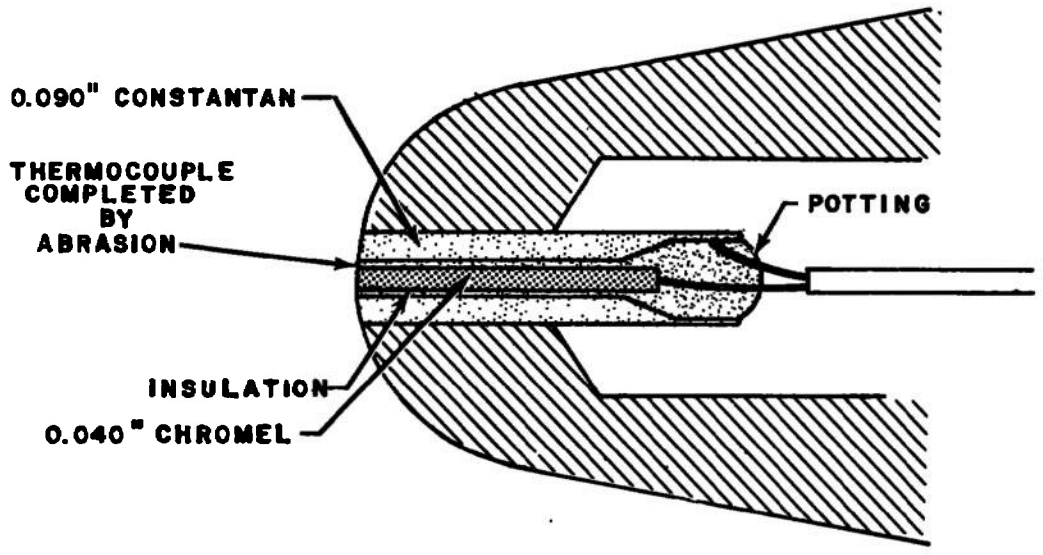

Fig. 11 Coaxial Thermocouple

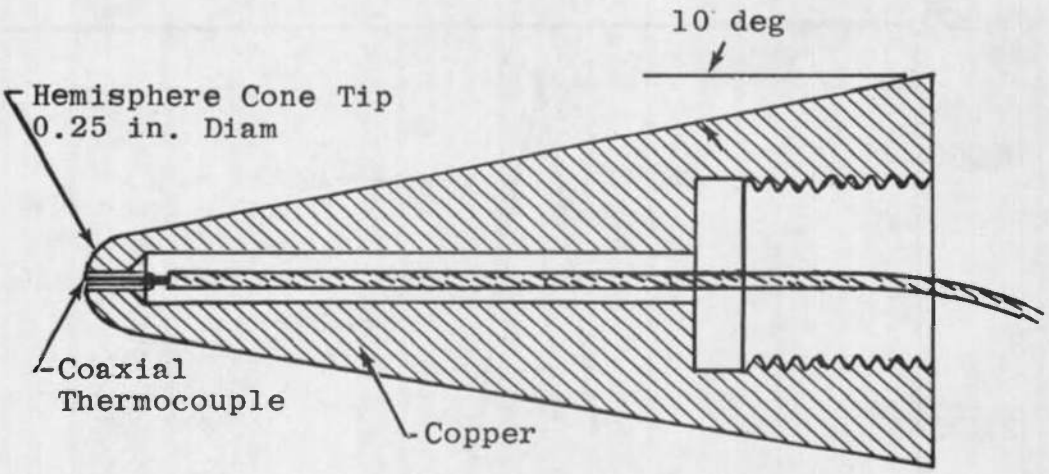

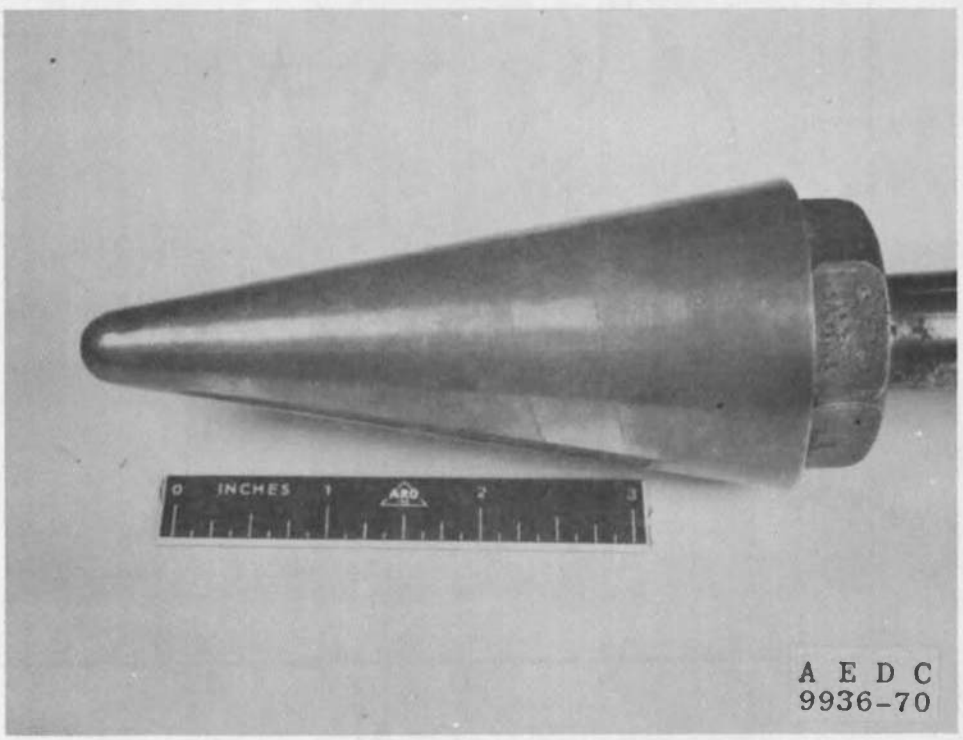

Fig. 12 Coaxial Thermocouple Stagnation Point Heat-Transfer Probe

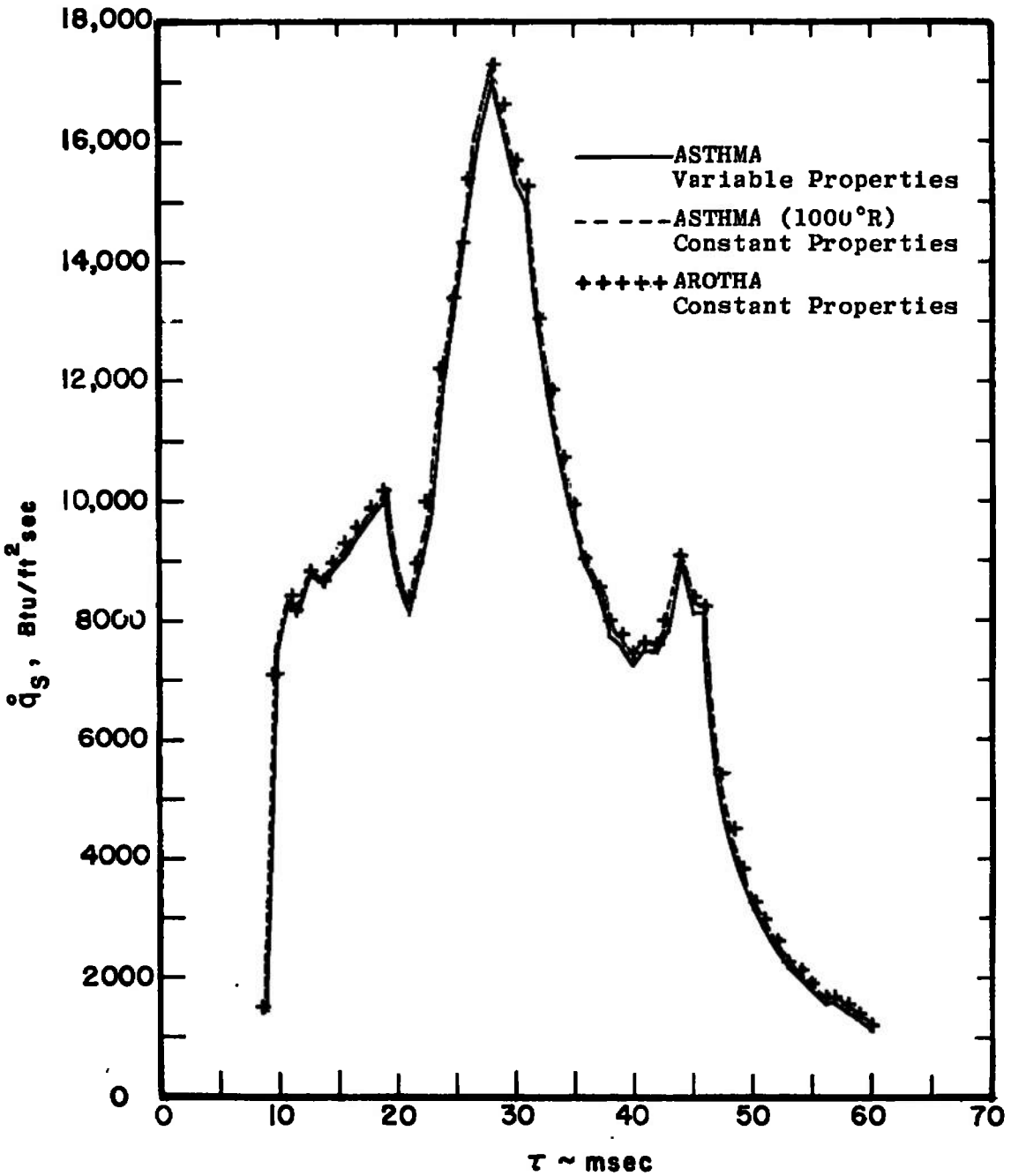

Fig. 13 Comparison of the Heat-Transfer Rate Calculated from AFFDL 50-MW Data by Two Data Reduction Programs

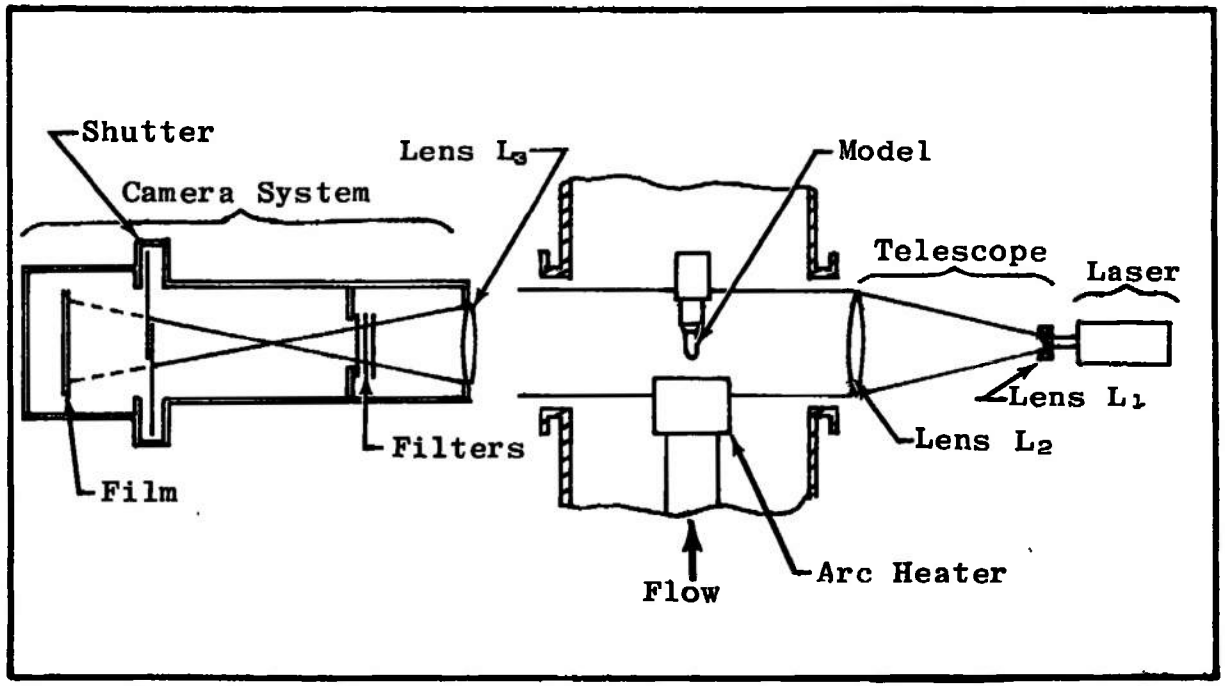

Fig. 14 Schematic of the Laser Shadowgraph System

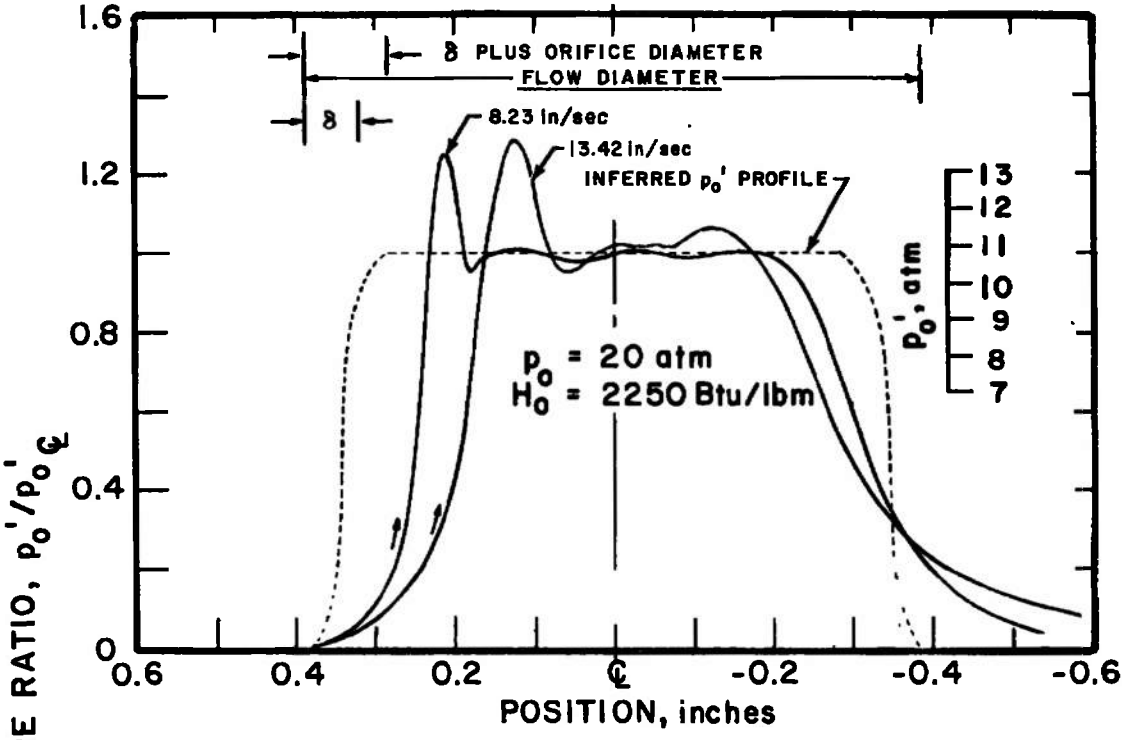

a. Graphite Tipped Probe, Oil Filled

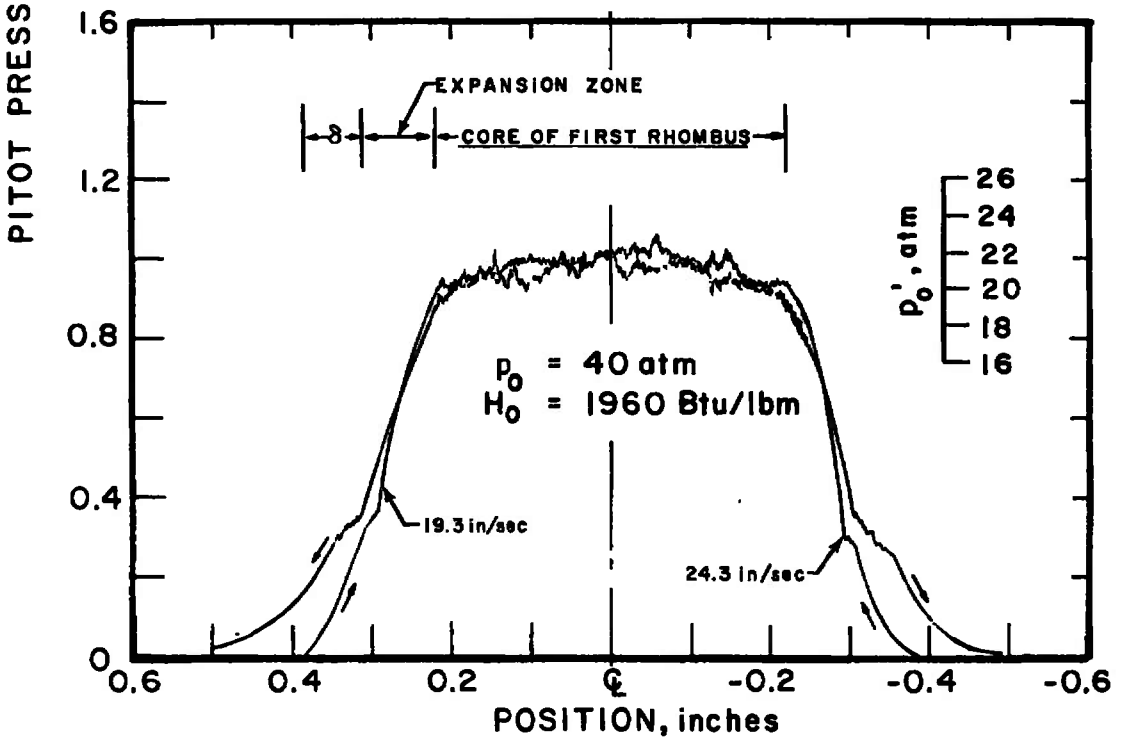

b. Boundary-Layer Probe

Fig. 15 Pitot Pressure Profiles Obtained with Various Total Pressure Probes

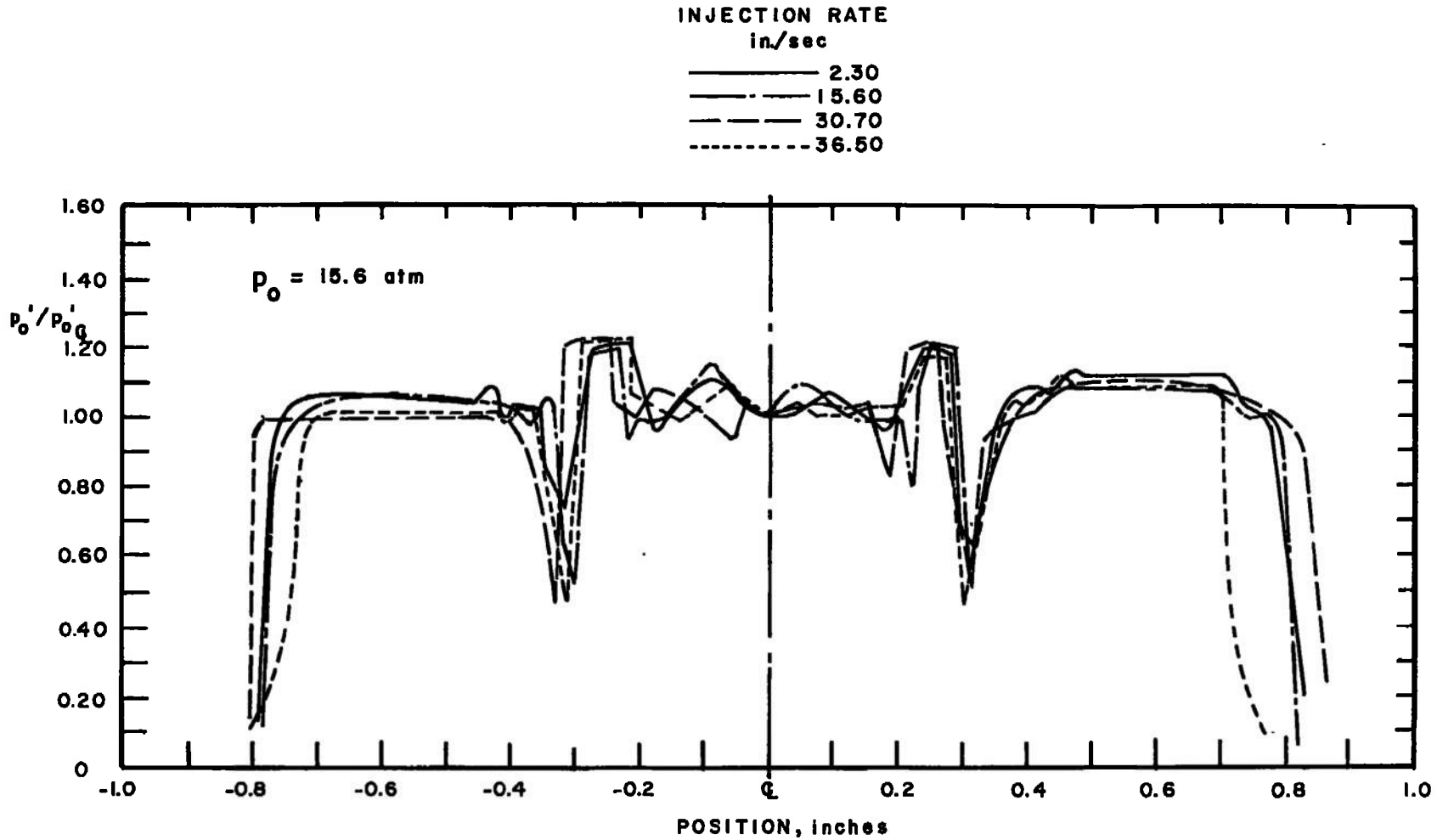

c. Improved Boundary-Layer Probe
Fig. 15 Concluded

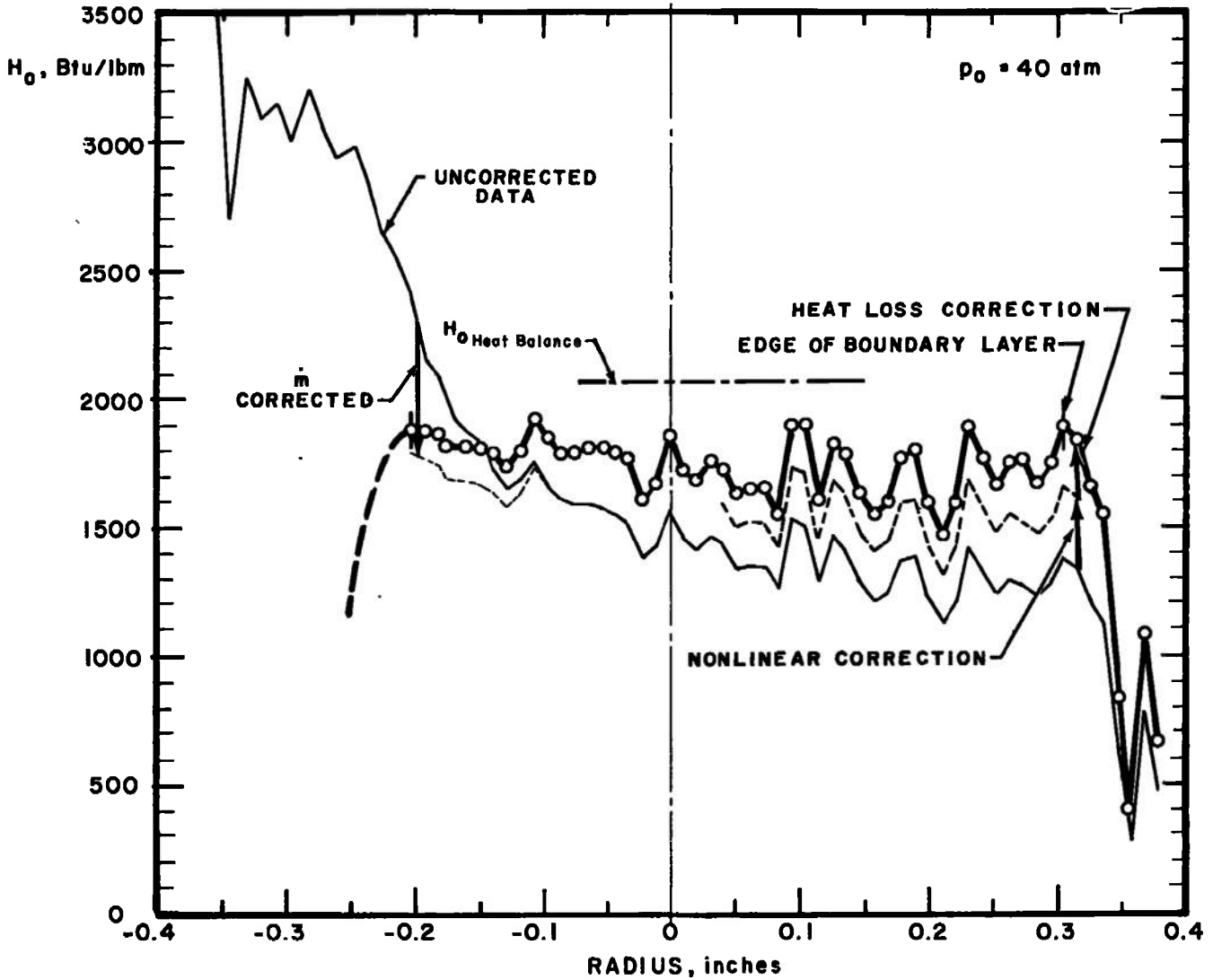

Fig. 16 Total Enthalpy Probe with Corrections

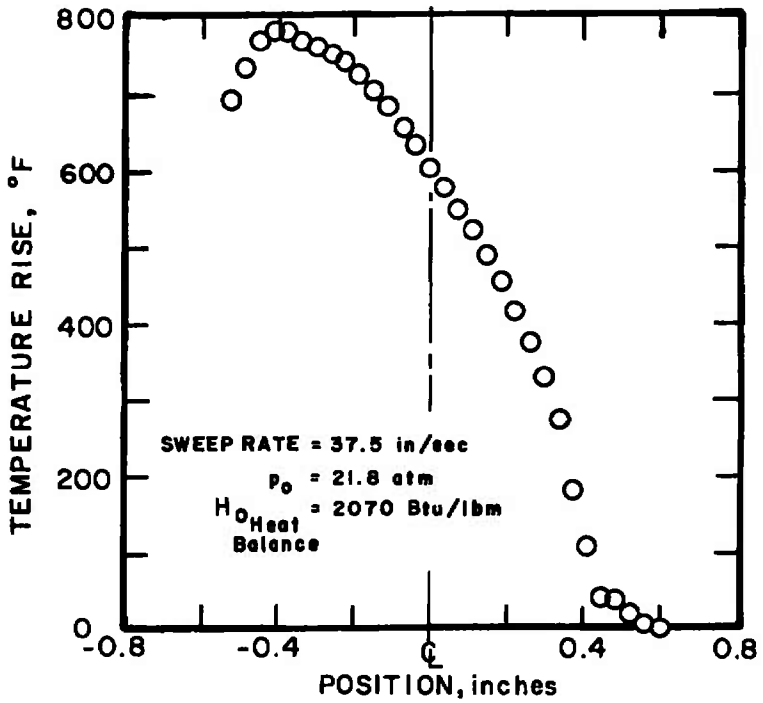

a. Coaxial Thermocouple Temperature

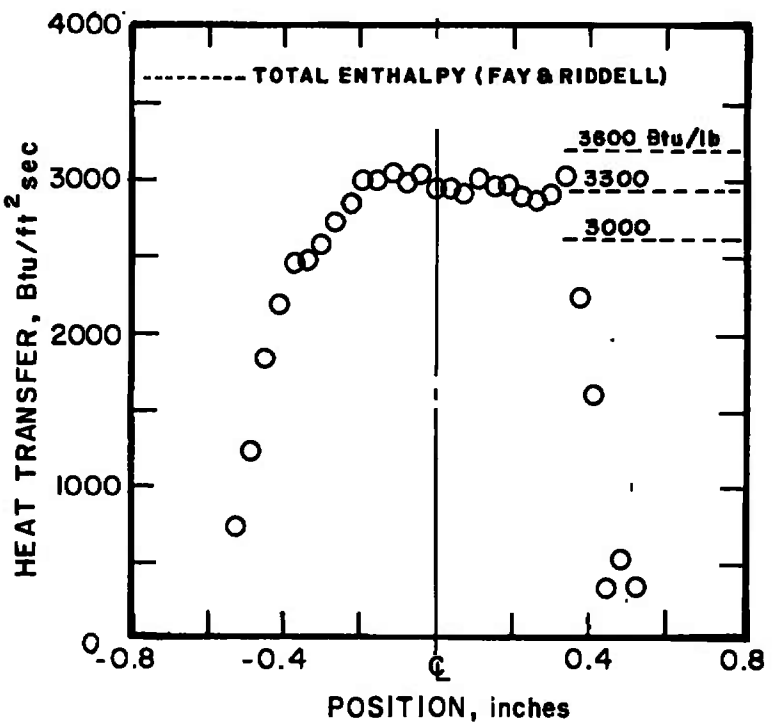

b. Heat-Transfer Rate and Enthalpy

Fig. 17 Typical Coaxial Thermocouple Stagnation Point Heat-Transfer Probe Data

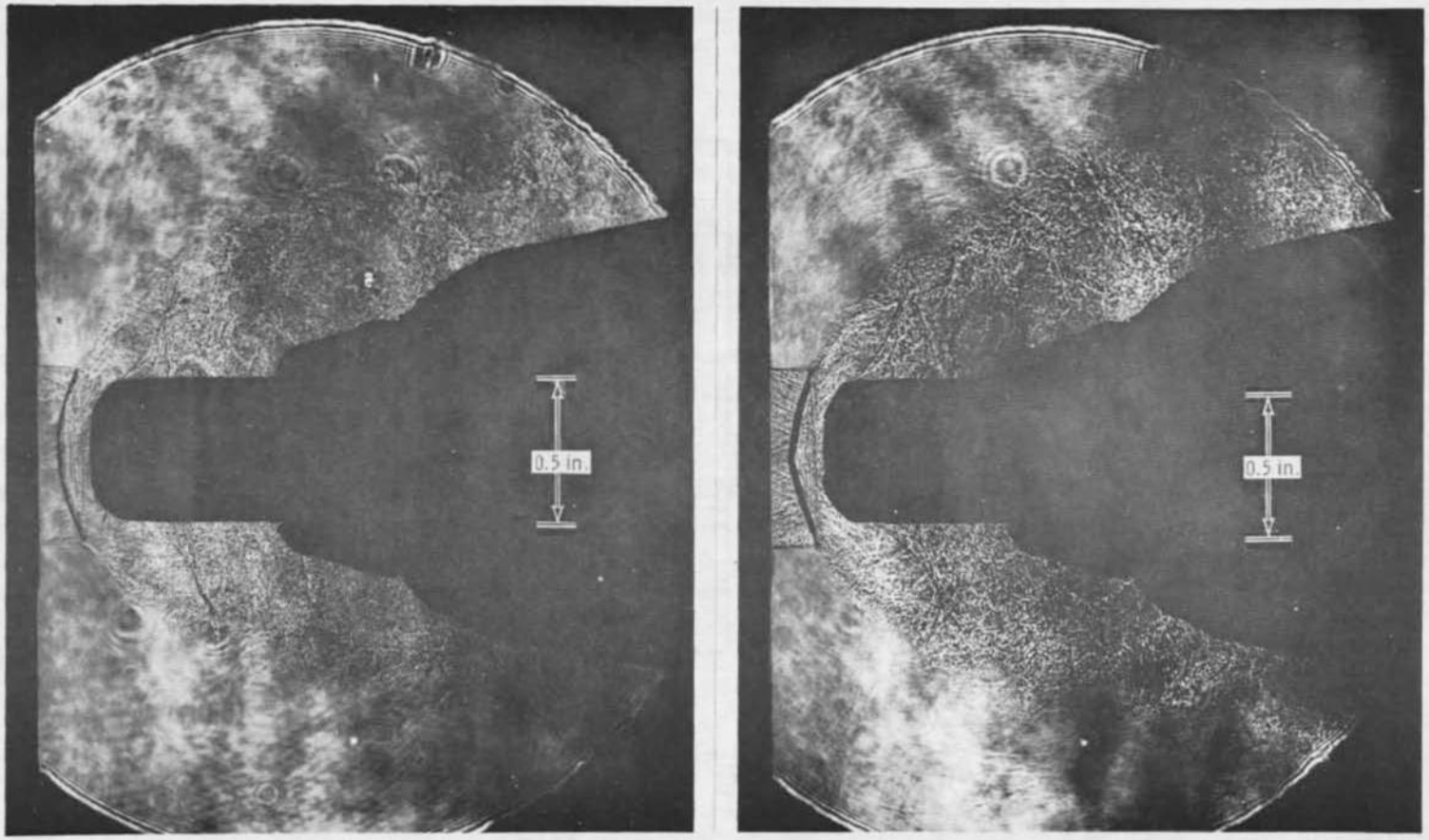

a. Image Plane on Centerline

b. Image Plane 1.0 in. from Centerline

Fig. 18 Effect of Varying Image Plane Location under Cold Flow Conditions with a Q-Switched Source

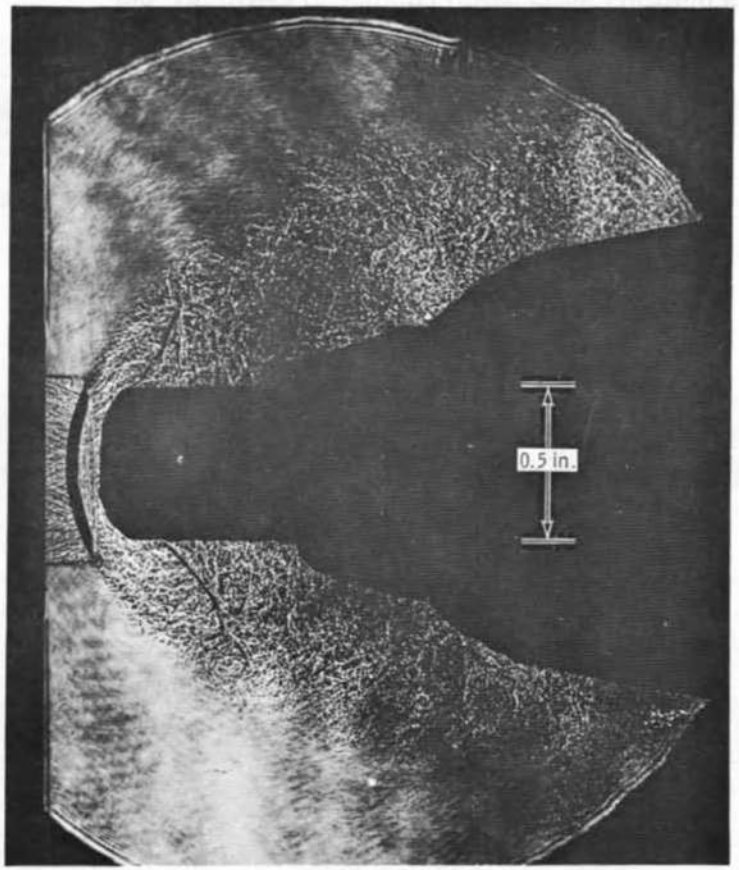

c. Image Plane 2.0 in. from Centerline

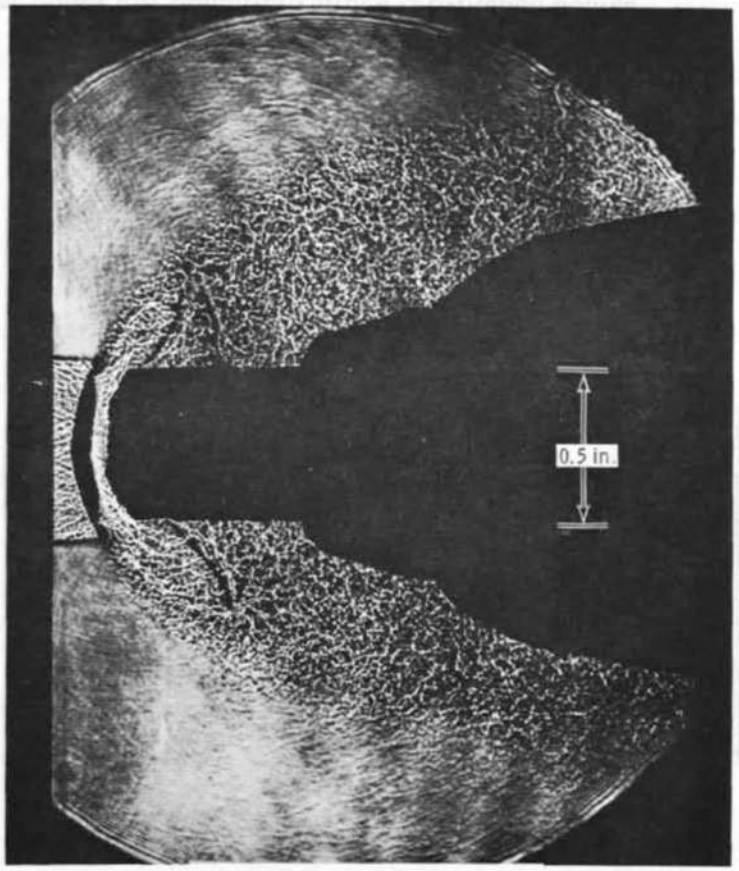

d. Image Plane 4.0 in. from Centerline

Fig. 18 Continued

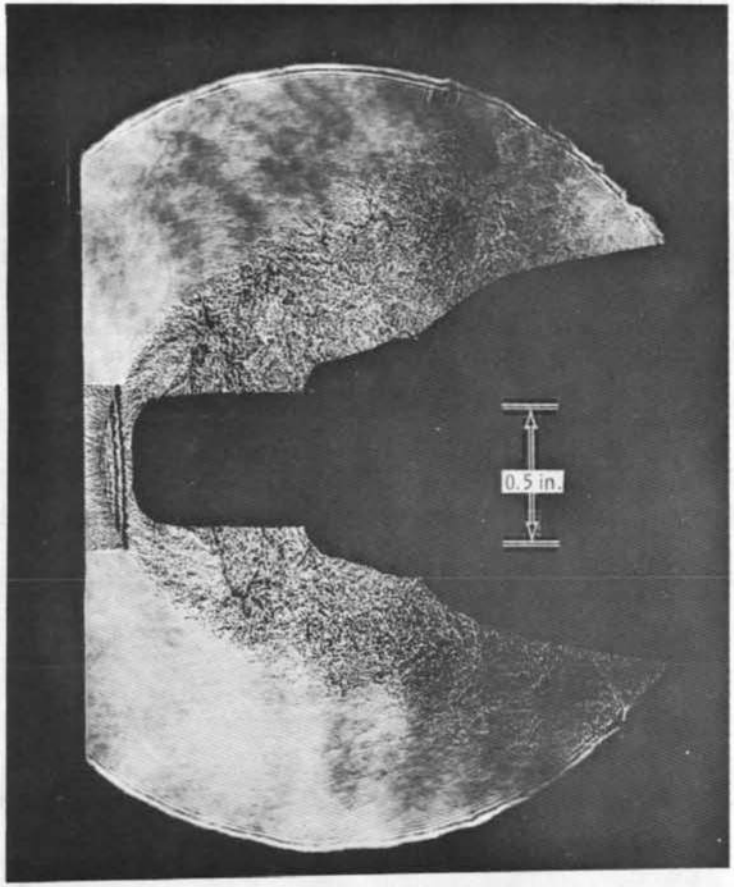

e. Image Plane 2.0 in. from Centerline toward Source

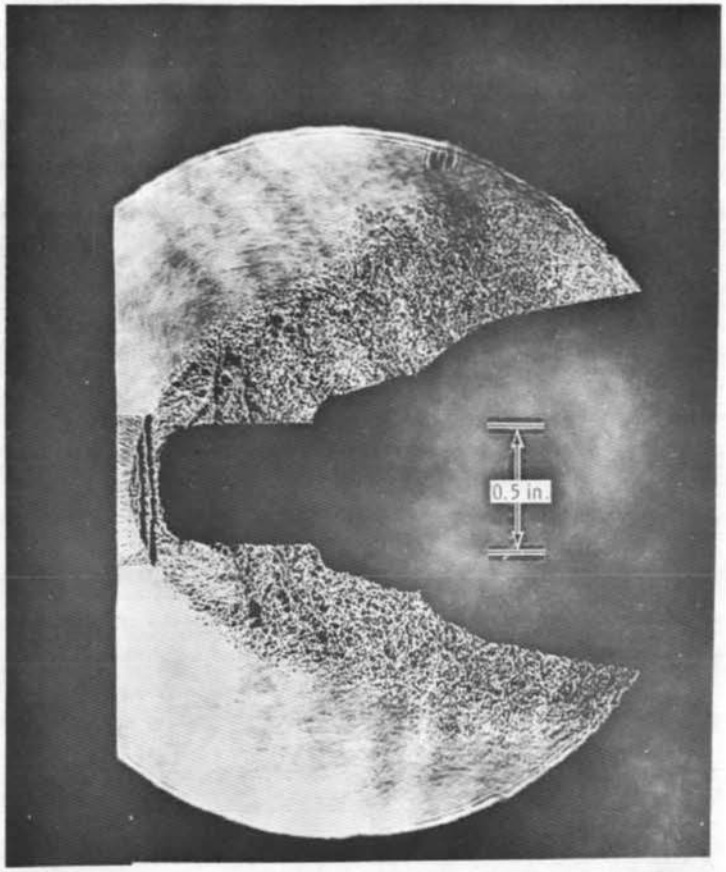

f. Image Plane 4.0 in. from Centerline toward Source

Fig. 18 Concluded

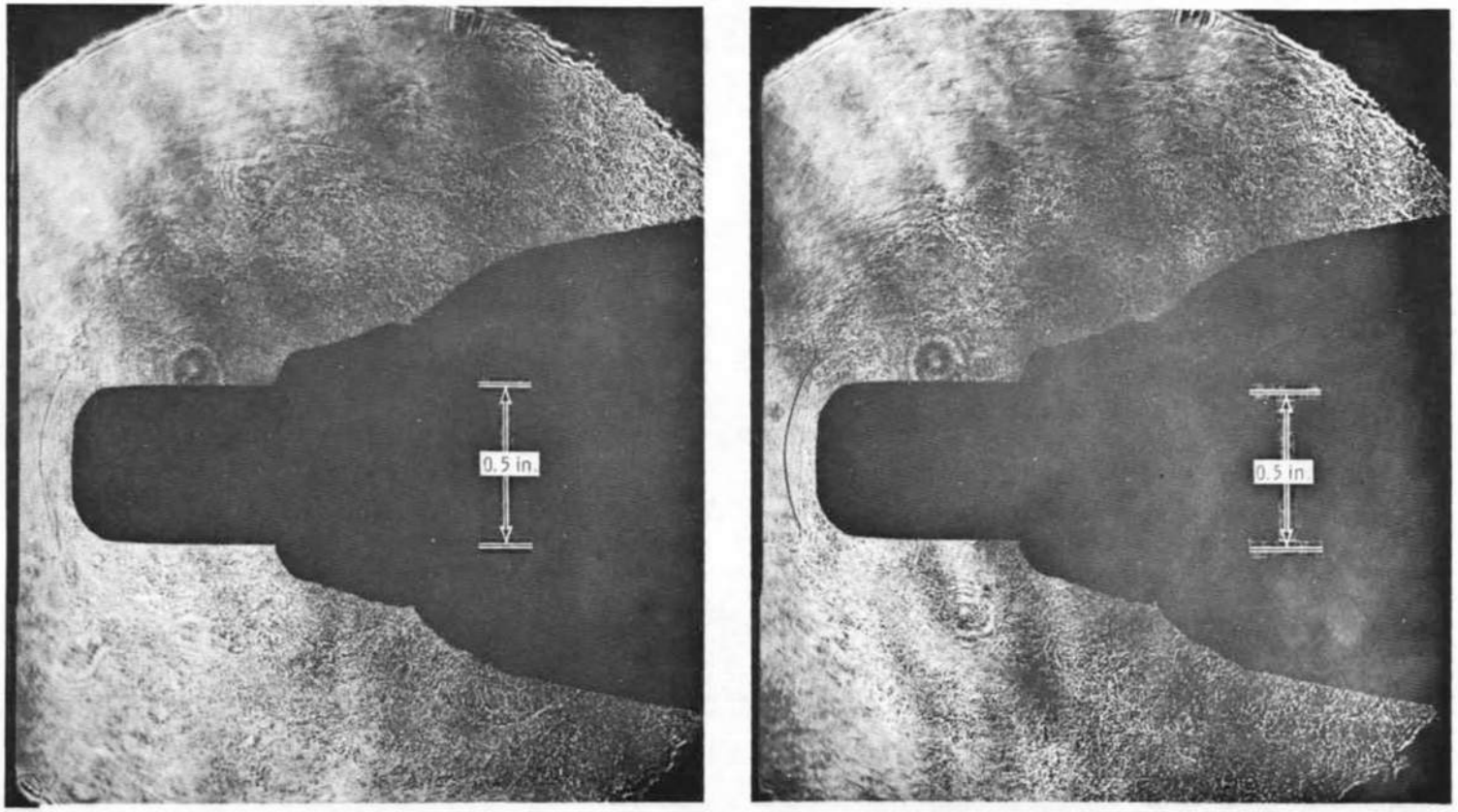

a. Image Plane on Centerline

b. Image Plane 0.5 in. from Centerline

Fig. 19 Effect of Varying Image Plane Locations under Hot Flow Conditions with a Q-Switched Source

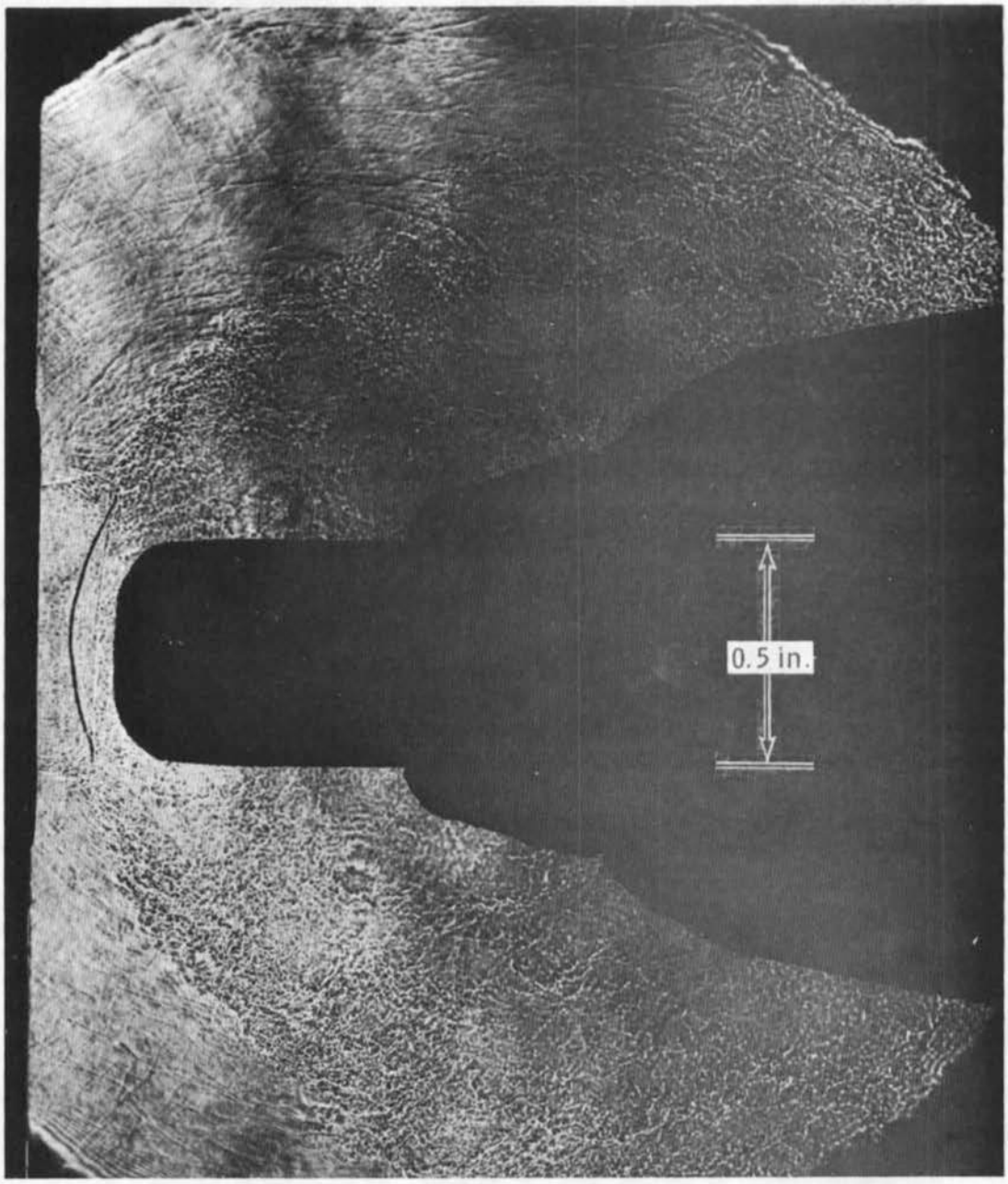

c. Image Plane 1.0 in. from Centerline
Fig. 19 Concluded

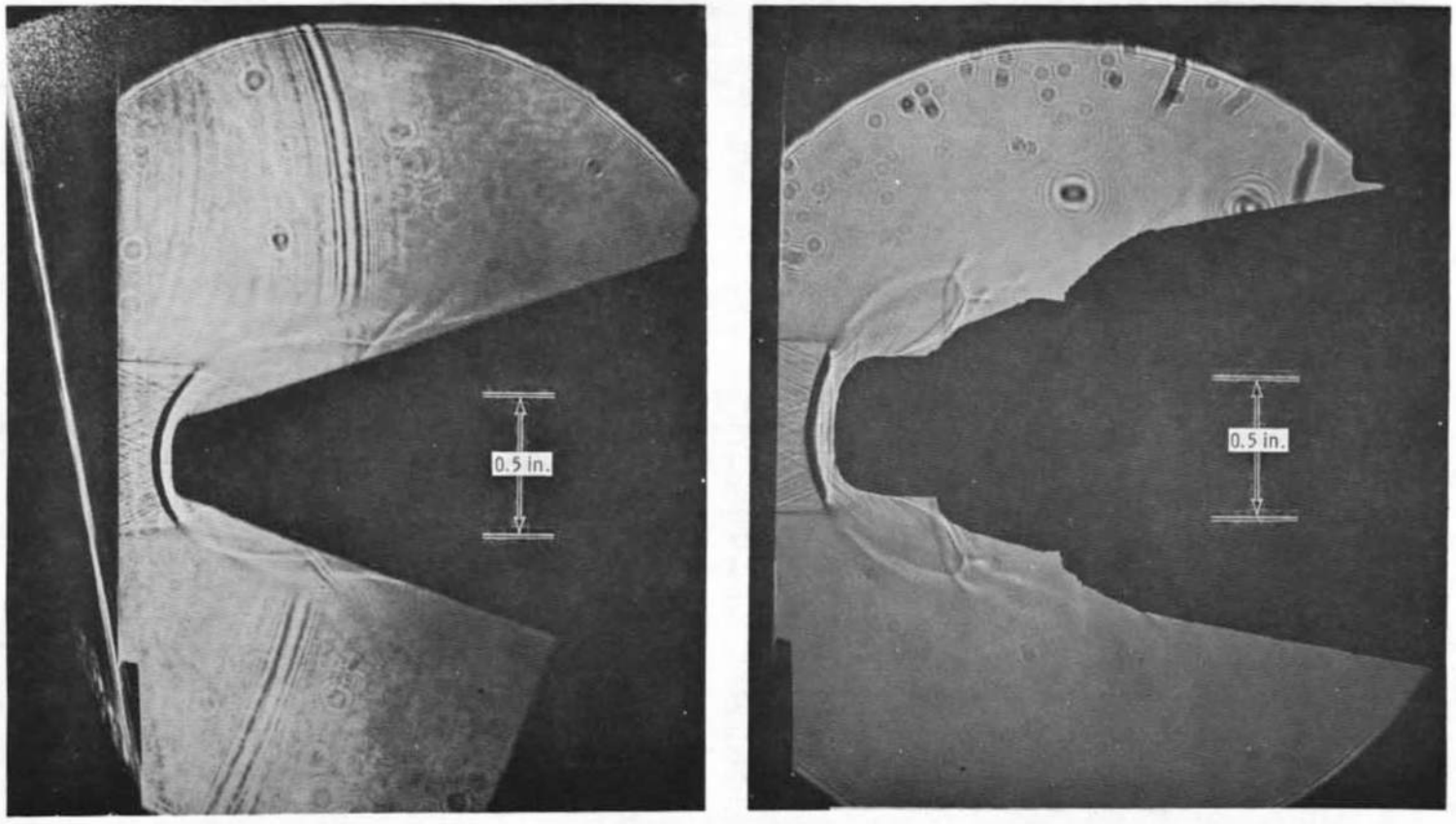

a. Normal Mode Source

b. Continuous Source

Fig. 20 Comparison of Light Sources under Cold Flow Conditions, Image Plane 2.0 in. from Centerline

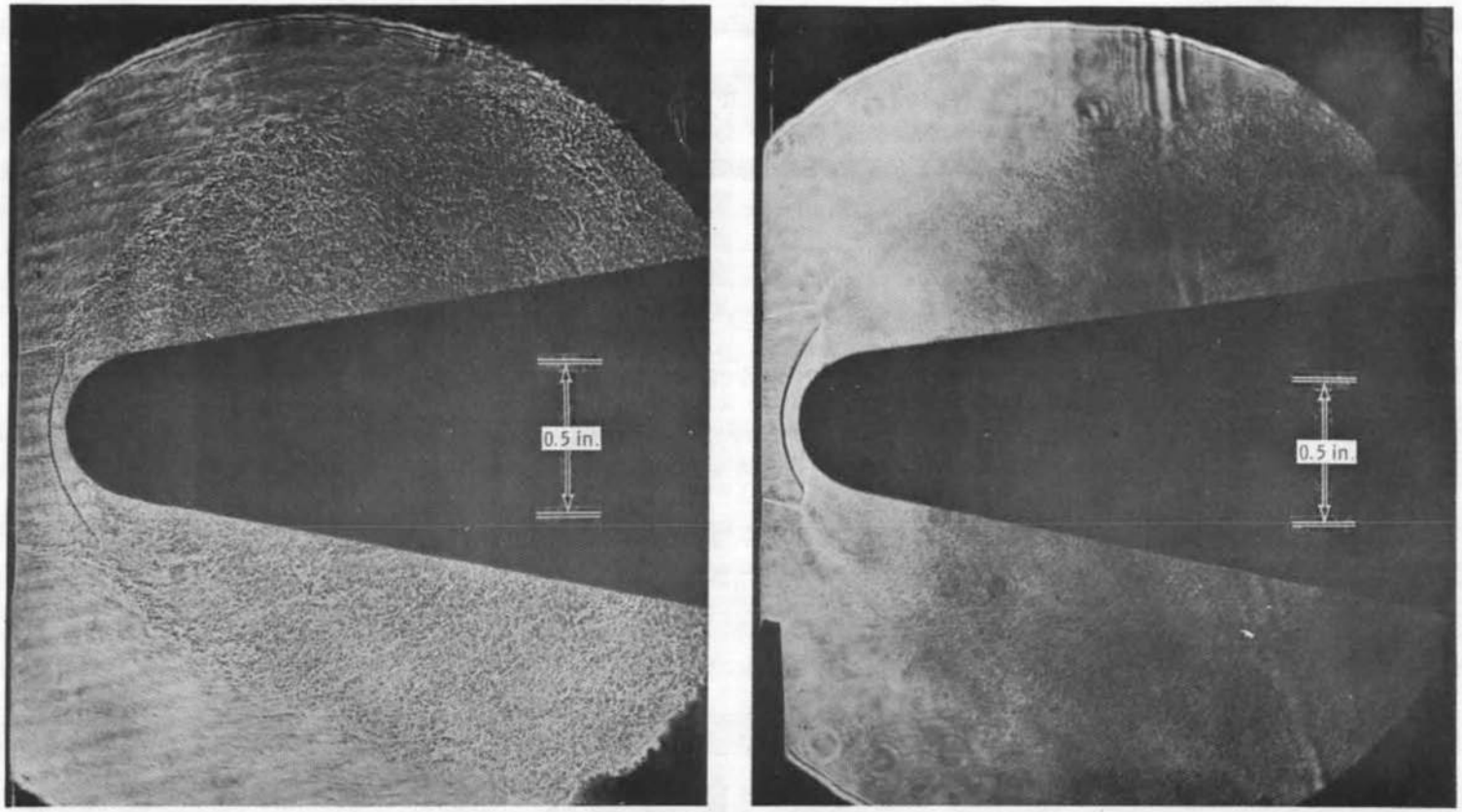

a. Q-Switched Source

b. Normal Mode Source

Fig. 21 Comparison of Light Sources under Hot Flow Conditions, Image Plane 2.0 in. from Centerline

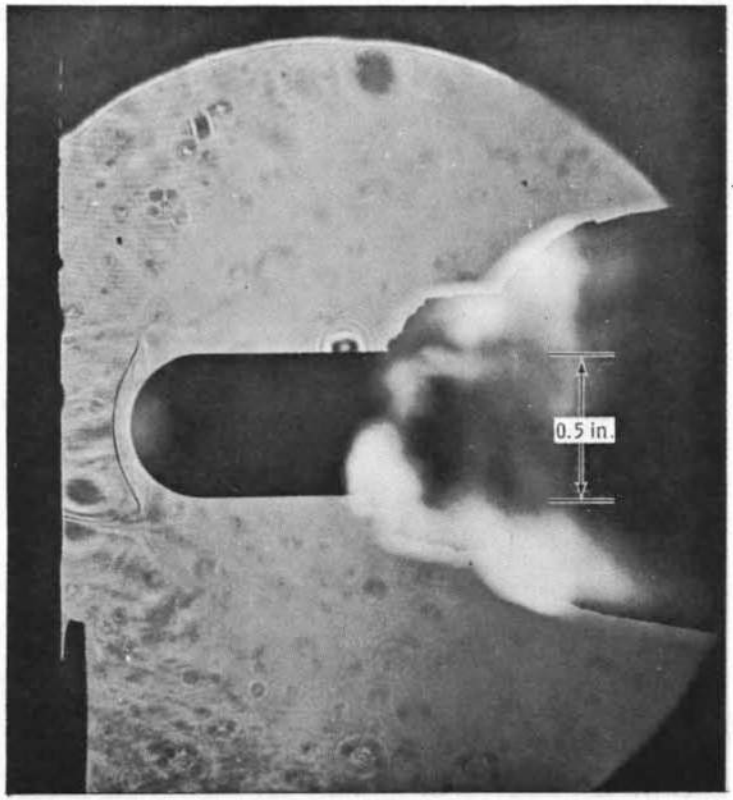

c. Continuous Source

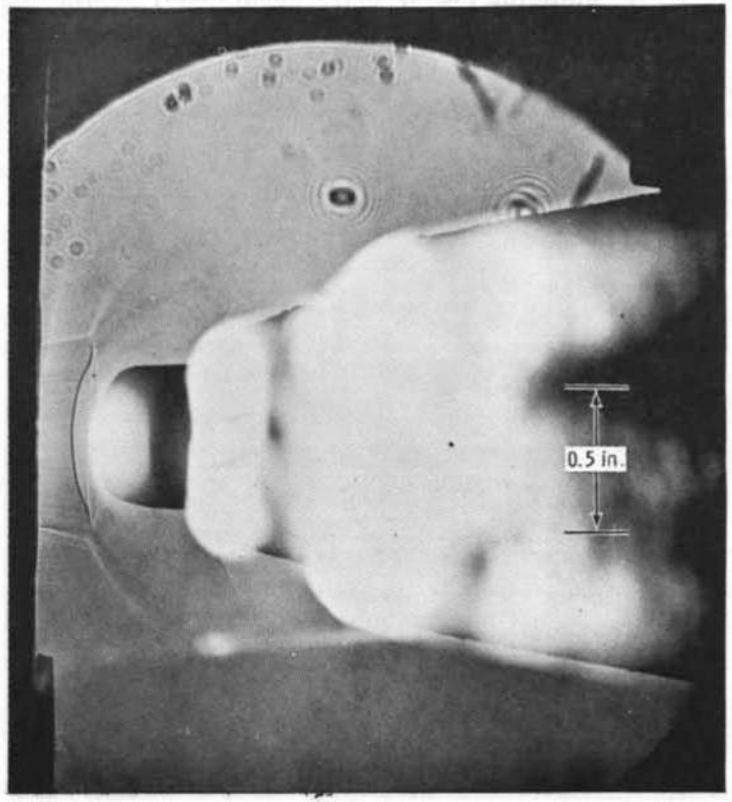

d. Continuous Source with Inadequate Filtering

Fig. 21 Concluded

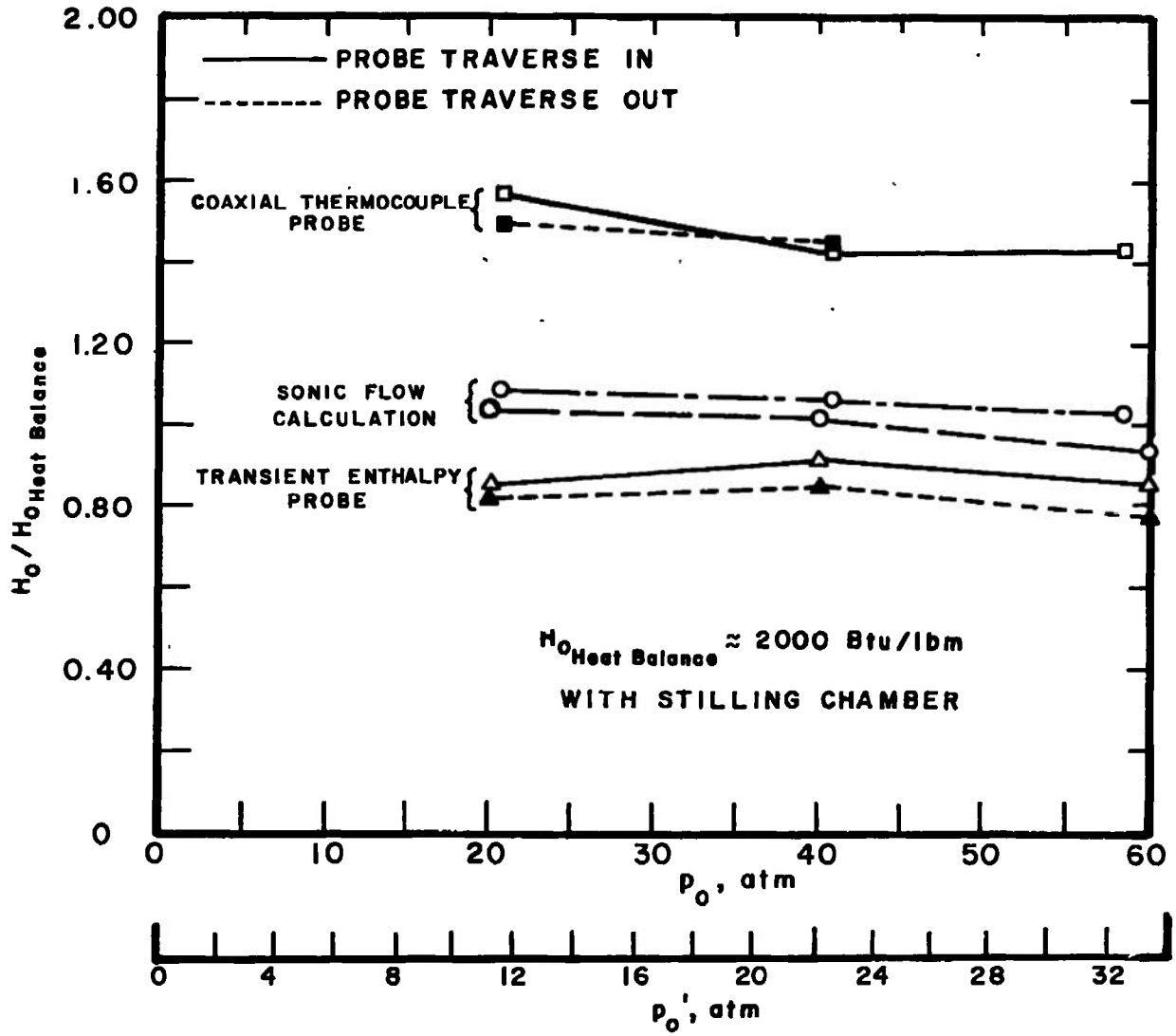

Fig. 22 Comparison of Four Methods of Total Enthalpy Measurement

TABLE I
LASER SPECIFICATIONS

Laser Description	Operation	Pulse Duration	Maximum Power	Energy	Beam Diameter	Wavelength
Universities Lab. He-Ne	Continuous	Continuous	4 mw	-	1.4 mm	6328Å
Korad K-1Q Ruby	Pulsed Mode	10-12 nsec	150 MW	1 joule	9/16 in.	6943Å
Korad K-1Q Ruby	Normal Mode	800 μsec	38 kw	30 joule	9/16 in.	6943Å

TABLE II
LENS DESCRIPTION

Lens Location	Lens Diameter, mm	Lens Focal Length, mm	A/R Coated	Lens Description
L_1	25	-100	Yes	Diffraction limited, 3 element, air-spaced Achromat
L_1	-	8	Yes	X20 microscope objective
L_2	152	1220	Yes	Good quality, 2 element, air-spaced Achromat
L_3	78	381	Yes	Good quality, 2 element, cemented Achromat

UNCLASSIFIED

Security Classification

DOCUMENT CONTROL DATA - R & D

(Security classification of title, body of abstract and indexing annotation must be entered when the overall report is classified)

1. ORIGINATING ACTIVITY (Corporate author)	2a. REPORT SECURITY CLASSIFICATION
Arnold Engineering Development Center ARO, Inc., Operating Contractor Arnold Air Force Station, Tennessee 37389	UNCLASSIFIED
	2b. GROUP N/A

3 REPORT TITLE

DEVELOPMENT OF CALIBRATION INSTRUMENTATION FOR ABLATION FACILITIES

4. DESCRIPTIVE NOTES (Type of report and inclusive dates)

Final Report, July 1970 to July 1971

5. AUTHOR(S) (First name, middle initial, last name)

J. C. Pigott, R. T. Smith, and W. N. MacDermott, ARO, Inc.

6. REPORT DATE	7a. TOTAL NO. OF PAGES	7b. NO. OF REFS
September 1971	58	7

8a. CONTRACT OR GRANT NO.	9a. ORIGINATOR'S REPORT NUMBER(S)
F40600-72-C-0003 b. PROJECT NO.	AEDC-TR-71-172
c. System 627A d. Program Element 63311F	9b. OTHER REPORT NO(S) (Any other numbers that may be assigned this report) ARO-PWT-TR-71-124

10. DISTRIBUTION STATEMENT

Approved for public release; distribution unlimited.

11 SUPPLEMENTARY NOTES	12. SPONSORING MILITARY ACTIVITY
Available in DDC.	Arnold Engineering Development Center, AFSC, Arnold Air Force Station, Tennessee 37389

13. ABSTRACT

Results are presented from a program conducted to develop calibration instrumentation for ablation facilities. The investigation included the development and evaluation of a transient total enthalpy probe, a stagnation point heat-transfer probe, and total pressure probes. A laser shadowgraph was developed for visualization of the flow field. Testing was conducted in the AEDC-PWT Arc Heater Test Unit (5 MW). Uncooled probes swept through the flow at high velocity (10 to 40 in./sec) survived the severe heat-transfer conditions and the desired data were obtained. The results of this investigation and a description of the calibration instrumentation are presented.

DD FORM 1 NOV 65 1473

UNCLASSIFIED

Security Classification

14. KEY WORDS	LINK A		LINK B		LINK C	
	ROLE	WT	ROLE	WT	ROLE	WT
test facilities						
1 electric arc						
2 ablation						
calibration						
enthalpy						
heat transfer						
pressure						

3. Ablation Test facilities